REPORT NO. ERR-SD-029

Antenna Group

A HELICAL MONOPULSE ANTENNA ARRAY

Willis E. Moore

13 December 1960

CONVAIR SAN DIEGO ELECTRONICS

ENGINEERING RESEARCH REPORT

CONVAIR SAN DIEGO CONVAIR DIVISION GENERAL DYNAMICS CORPORATION

60

ERR-SD-029
ANTENNAS GROUP

A HELICAL MONOPULSE ANTENNA ARRAY

Willis E. Moore

13 December 1960

Distribution Unlimited

CONVAIR-San Diego Electronics

ENGINEERING RESEARCH REPORT

This work was supported under Convair sponsored research program number 9905.

CONVAIR-San Diego
Electronics

A HELICAL MONOPULSE ANTENNA ARRAY

ABSTRACT

An array of four helical antennas connected through strip line hybrids to form a phase monopulse system, has been investigated to determine design criteria and limitations for such a system. The investigations included both theoretical and experimental work. Good agreement between experimental results and theoretical predictions was obtained. The basic design and characteristics of the system are described.

TABLE OF CONTENTS

		PAGE
I.	INTRODUCTION	1
II.	THE BASIC SYSTEM	1
III.	CHOICE OF PARAMETERS	2
IV.	MEASUREMENTS AND RESULTS	6
V.	CONCLUSIONS	9
VI.	RECOMMENDATIONS	10
VII.	REFERENCES	10
VIII.	ILLUSTRATIONS	11

FIGURE	ILLUSTRATIONS	PAGE
1	Circuit of four lobe monopulse system.	11
2	Development of monopulse radiation patterns	12
3	Geometry of an array of four sources	13
4	Coordinate System used in the measurements	14
5	Radiation patterns of a single helix	15
6	Four element helical array	16
7	Electrical circuit of strip line hybrids	17
8	Photograph of hybrids mounted behind array ground plane	18
9	Circuit for sum of two adjacent elements	19
10	Circuit for difference of two adjacent elements	19
11	Circuit for sum of sums patterns of four element array	20
12	Circuit for difference of sums patterns of four element array	20
13	Circuit for sum of sum and difference patterns of four element array	21
14	Circuit for difference of sum and difference patterns of four element array	21
15 - 19	Sum patterns, two elements fed in phase through a hybrid.	22-26
20 - 24	Difference patterns, two elements fed 180° in phase through a hybrid.	27-31
25 - 29	Sum of the sums patterns, four elements fed in phase through hybrids	32-36
30	Gain of four element helical array, all elements fed in phase.	37

FIGURE	ILLUSTRATIONS	PAGE
31 - 35	Difference of the sums patterns, two pairs of adjacent elements fed in phase, with pairs of elements fed 180° in phase	38-42
36 - 40	Sum of sum and difference patterns of four element array	43-47
41 - 45	Difference of sum and difference patterns of four element array	48-52
46	Direction finding sensing regions	53

I. INTRODUCTION

The purpose of this investigation was to determine criteria and limitations for a circularly polarized UHF four lobe phase monopulse antenna system of moderate directivity. Antenna systems of this type have found wide application inground tracking and telemetering receiving systems used in satellite and other missile tests. Other applications to aircraft flight test telemetering systems, tracking of drone aircraft and their location after flight, monitoring and locating of interfering sources of radio frequency radiation, and similar uses are possible.

A set of general characteristics sometimes specified for an antenna system of this nature is as follows:

Polarization: Circular, right hand

Gain of array with all elements in phase:
18 db or greater.

Frequency bandwidth: ± 14%

Direction finding sensitivity: ± 0.5 degrees.

Direction finding to be provided in both the horizontal and vertical planes.

With the above characteristics as a design objective, a program of theoretical and experimental investigations was initiated. Details of these investigations are described in the following sections of this report.

II. THE BASIC SYSTEM

The basic antenna system chosen for investigation was a square array of four helical antennas connected through hybrid couplers to form a phase monopulse system.

The helical elements were chosen because of their inherently broadband characteristics. When operating in the axial mode [1] the helical antenna produces a circularly polarized, moderately directive end-fire radiation pattern. The impedance of the antenna is essentially constant over a 2:1 frequency range, and the radiation pattern beamwidth remains essentially constant over a 1.7:1 frequency range.

Assembly of the helical radiating elements and connection of the elements through hybrid couplers may be best illustrated by reference to figure 1. The circuit employed is not the simplest possible; it is used because it provides approximately three db greater gain than the most simple type.

As illustrated in figure 1, signals from antenna elements 1 and 4 are routed to hybrid number I. Signals from antenna elements 2 and 3 are routed to hybrid number II.

The output of each of the antenna elements may be plotted as a function of horizontal and vertical directions as shown in figure 2a. The outputs of the sum channels of hybrids I and II are shown in figure 2b. Beam narrowing is achieved in the horizontal plane but not in the vertical plane. From the sum channel of hybrid III is obtained a pattern narrowed in both the horizontal and vertical planes. This pattern is the same as that which would be obtained by simply connecting all elements in phase. This pattern is shown in figure 2c. From the difference channel of hybrid III is obtained a split beam as shown in figure 2d. One major lobe is 90 degrees ahead and the other major lobe is 90 degrees behind the phase of the lobe from the sum channel of hybrid III. By inserting a 90 degree phasing line in the sum output of hybrid III, the relative phases of the lobes from the difference output may be made to be in a zero or 180 degree phase relationship with the lobe from the sum output. These signals from hybrid III are then routed through hybrid V. The outputs from hybrid V are anti-symmetric and when rectified produce a direct current output that indicates whether the arriving signal is up or down in direction from the axis of the antenna array. A very similar development will demonstrate the operation of the horizontal discriminator circuit.

III. CHOICE OF PARAMETERS

The choice of parameters depends upon the characteristics desired from the system. The directive gain of the system depends on the gain of the individual elements and also on the element spacing. The direction finding sensitivity of the system is also a rather complex function of these two factors. The control of extraneous lobes in the radiation patterns is one of the more important considerations determining the choice of parameters, since these extraneous lobes can create ambiguities in direction finding. The analysis that follows points up some of the more important factors in arriving at the parameters chosen for experimental investigation.

To start the analysis, we may consider the radiation pattern of four radiators disposed as in figure 3. Assume all radiators have identical patterns and are fed with equal amplitude voltages. Also assume the radiators are equally spaced a distance $\underline{a}_o$ to form a square with vertices at $\phi = 45^\circ, 135^\circ, 225^\circ$ and 315°.

From source 1

$$E_1 = E_0 e^{j(\omega t - \frac{R}{c})} e^{j\left(\frac{\sqrt{2}\pi a}{\lambda} \sin\theta \cos\left(\phi - \frac{\pi}{4}\right)\right)}$$

From source 3

$$E_3 = E_0 e^{j(\omega t - \frac{R}{c})} e^{-j\left(\frac{\sqrt{2}\pi a}{\lambda} \sin\theta \cos\left(\phi - \frac{\pi}{4}\right)\right)}$$

From source 2

$$E_2 = E_0 e^{j(\omega t - \frac{R}{c})} e^{j\left(\frac{\sqrt{2}\pi a}{\lambda} \sin\theta \cos\left(\phi - \frac{3\pi}{4}\right)\right)}$$

From source 4

$$E_4 = E_0 e^{j(\omega t - \frac{R}{c})} e^{-j\left(\frac{\sqrt{2}\pi a}{\lambda} \sin\theta \cos\left(\phi - \frac{3\pi}{4}\right)\right)}$$

Dropping the time retardation factor $e^{j(\omega t - \frac{R}{c})}$ and defining: $E \equiv f(\theta, \phi)$

$$\gamma = \frac{\sqrt{2}\pi a}{\lambda} \sin\theta \cos\left(\phi - \frac{\pi}{4}\right)$$

$$\delta = \frac{\sqrt{2}\pi a}{\lambda} \sin\theta \cos\left(\phi - \frac{3\pi}{4}\right) = \frac{\sqrt{2}\pi a}{\lambda} \sin\theta \sin\left(\phi - \frac{\pi}{4}\right)$$

we obtain

$$E_1 = f(\theta, \phi)\, e^{j\gamma}$$

$$E_2 = f(\theta, \phi)\, e^{j\delta}$$

$$E_3 = f(\theta, \phi)\, e^{-j\gamma}$$

$$E_4 = f(\theta, \phi)\, e^{-j\delta}$$

For in-phase excitation of all sources, the total field

$$E \text{ (in phase)} = [f(\theta, \phi)][e^{j\gamma} + e^{-j\gamma} + e^{j\delta} + e^{-j\delta}]$$

$$= 2[f(\theta, \phi)][\cos\gamma + \cos\delta]$$

The radiation intensity $U \equiv K|E^2|$

$$U \equiv 4K[f(\theta,\phi)]^2[\cos\gamma + \cos\delta]^2$$

For $\phi = \frac{n\pi}{2}$, $n = 0, 1, 2, \cdots\cdots$

$$E_{\phi=\frac{n\pi}{2}} = 4[f(\theta, \phi)]\left[\cos\left(\frac{\pi a}{\lambda}\sin\theta\right)\right]$$

$$U_{\phi=\frac{n\pi}{2}} = 16K[f(\theta, \phi)]^2\left[\cos^2\left(\frac{\pi a}{\lambda}\sin\theta\right)\right]$$

For $\phi = \frac{n\pi}{2} \pm \frac{\pi}{4}$, $n = 0, 1, 2, \cdots\cdots$

$$E_{\phi=\frac{n\pi}{2}\pm\frac{\pi}{4}} = 4[f(\theta, \phi)]\left[\cos^2\left(\frac{\pi a}{\sqrt{2}\lambda}\sin\theta\right)\right]$$

$$U_{\phi=\frac{n\pi}{2}\pm\frac{\pi}{4}} = 16K[f(\theta, \phi)]^2\left[\cos^4\left(\frac{\pi a}{\sqrt{2}\lambda}\sin\theta\right)\right]$$

Nulls in the pattern at $\phi = \frac{n\pi}{2}$ occur when $\cos\left(\frac{\pi a}{\lambda}\sin\theta\right) = 0$

or when

$$\frac{a}{\lambda} = \pm\left(\frac{n + \frac{1}{2}}{\sin\theta}\right)$$

or when

$$\sin\theta = \pm\frac{1}{\frac{a}{\lambda}}\left(n + \tfrac{1}{2}\right)$$

For sources 1 and 2 fed in phase and sources 3 and 4 fed 180° in phase with sources 1 and 2, the total field

$$E_{(diff.)} = \left[f(\theta, \phi)\right]\left[e^{j\gamma} - e^{-j\gamma} + e^{j\delta} - e^{-j\delta}\right]$$

$$= j\,2\left[f(\theta, \phi)\right]\left[\sin\gamma + \sin\delta\right]$$

The radiation intensity

$$U = 4k\left[f(\theta, \phi)\right]^2\left[\sin\gamma + \sin\delta\right]^2$$

For $\phi = n\pi$,

$$E_{\phi = n\pi} = U_{\phi = n\pi} = 0$$

For $\phi = n\pi + \frac{\pi}{2}$,

$$E_{\phi = n\pi + \frac{\pi}{2}} = j\,4(-1)^n\left[f(\theta,\phi)\right]\left[\sin\left(\frac{\pi a}{\sqrt{2}\lambda}\sin\theta\right)\right]$$

$$U_{\phi = n\pi + \frac{\pi}{2}} = 16\left[f(\theta,\phi)\right]^2\left[\sin^2\left(\frac{\pi a}{\sqrt{2}\lambda}\sin\theta\right)\right]$$

Nulls in the pattern at $\phi = n\pi + \frac{\pi}{2}$ occur when

$$\sin\left(\frac{\pi a}{\sqrt{2}\lambda}\sin\theta\right) = 0$$

or when

$$\sin\theta = \pm\frac{\sqrt{2}\,n}{\frac{a}{\lambda}}$$

or when

$$\frac{a}{\lambda} = \pm\frac{\sqrt{2}\,n}{\sin\theta}$$

The foregoing analysis shows that array factor nulls for the system with all elements in phase (sum of sums arrangement) are interspersed between array factor nulls for the system with two elements 180° in phase with respect to the other two elements (difference of sums arrangement). The first array factor null for the difference arrangement occurs at $\theta = 0^{o}$, for $n = 0$. The first array factor null for the sum arrangement occurs for $n = 0$, and the angle θ at which it occurs depends on the element spacing a.

The resulting pattern of the array depends on the element spacing and also on the primary pattern $f(\theta, \phi)$ of each element. It is desirable to use a large element spacing insofar as achieving high antenna gain and direction finding sensitivity are concerned. On the other hand, too large a spacing of elements results in excessively large side lobes. These large side lobes decrease the performance on the system by creating ambiguities inthe direction finding discrimination. A compromise in array factor is therefore required. It is ordinarily the practice to design the array with a spacing such that first order nulls of the array factor occur at angles corresponding to those of the peaks of the first side lobes of the element pattern. In this way low side lobe levels in the complete array pattern are achieved. This procedure, however, is not necessarily optimum in producing highest gain for a given array size. It requires that thegain of each element be greater than a certain minimum value, if a given overall gain is tc be achieved. For the particular array gain values desired, this procedure would require excessively long helical elements to obtain the required element gain. This creates mechanical problems in supporting the helical elements and in obtaining a good form factor for the array. For this reason a different compromise in choice of array factor and element gain was made. The design constants for this compromise were chosen after radiation pattern measurements on a single helical element were performed.

Kraus[1] provides basic design data for the helical elements. It was desirable that as much of the array gain as possible be produced by the individual elements to minimize side lobe levels. Limitations imposed on the length of the elements by mechanical support considerations, however, dictated that shorter than optimum elements be used. The element configuration finally chosen was a 10 turn helix with a 12° pitch angle. Radiation pattern measurements were made using this configuration.

MEASUREMENTS AND RESULTS

For convenience, experimental work was performed at L-band frequencies. Radiation patterns were first performed on a single helical element having the following parameters:

D = diameter of helix = 2.88 inches.

C = circumference of helix in wavelengths = 1.07 at 1400 mc

P = pitch of helix = 12°

N = number of turns = 10

d = wire diameter = .072 inch

H = overall element height = 19.23 inches

The helix element was mounted on a 4.8 inch square plane and supported by a brass pipe of .5 inch diameter 19.75 inches long. Wooden support spars were placed at 120° intervals around the support pipe to hold the helix element rigidly in place. Construction was similar to that shown in the photograph of the four element array, figure 6.

The coordinate system used in the radiation pattern measurements is illustrated in figure 4.

Radiation patterns of the single helix are shown in figure 5. These radiation patterns were made at 1500 mc. using linear polarization. The axial ratio of the helix was 1.12 db. The half power beam width was approximately 34°. The gain was 10.88 db for linear polarization, or 13.88 db for circular polarization.

From a study of the radiation patterns of the single helix, the array geometry was determined. A first null location at $\theta = 17^\circ$ was chosen for the sum pattern (all elements in phase) of the array as an optimum compromise for good sensitivity and low side lobe levels. This corresponded to an element spacing of 1.72 wavelengths (14.5 inches) at the mid frequency of 1400 mc for the model used. This choice dictated the location for the second null (the first null away from $\theta = 0^\circ$) of the difference pattern (two adjacent elements in phase and the other two elements 180° in phase with the first two). The location of that null may be calculated to be at $\theta = 55^\circ$.

An array with 14.5 inches element spacing was constructed. Preliminary tests with the first array indicated that currents were being formed on the outside of feed lines and as a result unpredictable radiation patterns were produced. Accordingly, a large square ground plane 28.8 inches on each side was constructed, upon which the antenna elements were mounted. Radiation patterns taken on this model showed good agreement with theory. This array is shown in figure 6.

Sum and difference radiation patterns were obtained by interconnecting the antennas with simple strip line hybrid couplers. These couplers were of the $\lambda/4$, $\lambda/4$, $\lambda/4$, 3 $\lambda/4$ "ratrace" type for simplicity in construction. No particular effort was made to achieve balance at frequencies away from the center frequency of 1400 mc. A sketch showing the electrical circuit of the hybrid is shown in figure 7. A photograph of the hybrids mounted on the rear of the array ground plane is shown in figure 8.

The complete circuitry of the system was somewhat complex. For this reason radiation patterns were measured for subassembly portions of the circuit to illustrate the basic functional operation of each portion of the circuit. Measurements were made using a circularly polarized source (actually the model upon which the single element radiation patterns were measured).

Measurements were made for the following conditions:

1. Sum patterns of elements 1 and 4 connected in phase through a hybrid. Elements 2 and 3 terminated in 50 ohms. Circuit of figure 9. These patterns are shown in figures 15 through 19.

2. Difference patterns of elements 1 and 4 connected 180° in phase through a hybrid. Elements 2 and 3 terminated in 50 ohms. Circuit of figure 10. These patterns are shown in figures 20 through 24.

3. Sum of sums patterns of four element array. Circuit of figure 11. These patterns are shown in figures 25 through 29.

4. Difference of sums patterns of four element array. Circuit of figure 12. These patterns are shown in figures 31 through 35.

5. Sum of sum and difference patterns of four element array. Circuit of figure 13. These patterns are shown in figures 36 through 40.

6. Difference of sum and difference patterns of four element array. Circuit of figure 14. These patterns are shown in figures 41 through 45.

The patterns of two elements connected in phase, figures 15 through 19, show the effect of the in-phase arraying of the elements. The ϕ = 0° patterns are not affected by the arraying. The ϕ = 90° patterns show the beam narrowing with nulls at the predicted angle of θ = 17° at 1400 mc. The balance of the hybrid was found to be quite good over the entire frequency band from 1200 mc to 1600 mc, as evidenced by the depth of pattern nulls which were greater than 20 db below the beam maximum throughout the band. The effect of compromising on the gain of individual elements is shown by the size of side lobes in the ϕ = 90° patterns.

The patterns of two elements connected 180° in phase, figures 20 through 24, show good agreement with theoretical calculations. Some of the ϕ = 0° patterns show a sizeable signal strength at θ = 0°. This is accounted for by the backlash in the gearing of the model tower mount, which has a nominal 1/4 degree positioning accuracy. The steep slope of the pat-

tern about $\theta = 0^{o}$ requires a greater accuracy for faithful reproduction of patterns in the area of the null than was possible with the model tower mount used. This deficiency was not, however, considered of prime importance in this investigation.

The sum of the sums patterns, figures 25 through 29, show the results of feeding all four elements in phase. These patterns again illustrate the high side lobe levels occasioned by restrictions on the size, and hence the directivity, of the individual elements of the array. A complete set of patterns of all elements fed in phase by simple parallel connection of the elements was measured, but is not included in this report because of the large number of individual patterns. From those patterns, which were essentially identical to those of figures 25 through 29, the gain of the array was calculated. Figure 30 shows the gain of the array throughout the frequency band.

The difference of the sums patterns, figures 31 through 35, show good null depth at $\theta = 0^{o}$, indicating good symmetry in construction of the array and hybrids and in transmission line cabling. The sum of sum and difference patterns, figures 41 through 45, illustrate the nature of direction-finding sensing voltages produced by the array.

The effect of limiting the size and directivity of individual elements is particularly apparent in these patterns. The effect of the large side lobe level is to introduce a region wherein reverse direction finding sensing occurs. An ambiguity in pointing is also introduced as a result of the reverse direction finding. This condition is perhaps best illustrated in the graph, figure 46.

The reverse sensing region and sensing ambiguity somewhat reduce the performance of the system; by proper operational procedures, however, their effects may be minimized. If, when acquiring a target, the antenna is oriented so that a maximum signal is received from the sum of the sums terminal (this represents the condition of all elements fed in phase), the antenna will then be oriented within the region of proper direction finding sensing.

As an operational test, the antenna was connected with a complete sensing system for one plane of direction finding. Measurements were made to determine the accuracy and consistency of direction finding properties throughout the frequency band. It was found that the sensitivity of direction finding was limited by the accuracy of the mount which held the antenna. This accuracy was approximately 1/4 degree. Some pointing error, up to a maximum of about two degrees, was noted. This error may be attributed to inaccuracies in cable lengths and to unbalance in the hybrids. For an operational unit, with due exercise of care in design and construction, these inaccuracies would be greatly decreased with consequent improvement in pointing accuracy.

V. CONCLUSIONS

The basic design parameters for a UHF four lobe phase monopulse antenna system utilizing circular polarization have been investigated. A basic

design has been developed that meets the requirements described in the introduction. This basic design may be applied to systems operating at other frequencies or, by slight modification, to systems having somewhat different characteristics.

An advantage of the design chosen is its relatively small size and simplicity. It lends itself readily to the construction of a portable modular type antenna array which can be easily assembled or disassembled.

A disadvantage of the design chosen is the limitation imposed upon the gain of individual elements by mechanical considerations. This reduces the angular region in which proper direction finding sensing occurs. This condition could be improved by the use of more individual elements, connected in parallel, to give higher equivalent element gains. The benefits to be derived from such a design change are in most cases offset by the greater complexity of the system.

VI. RECOMMENDATIONS

This investigation has resulted in the development of an antenna design which has wide application in such fields as telemetry, aircraft or missile tracking, and the detection, locating and monitoring of sources of radio frequency radiation. A large potential market for antenna designs of this type exists, and it is recommended that an aggressive effort to exploit this market be made.

VII. REFERENCES

1. J. D. Kraus, "Antennas", 1st ed., McGraw-Hill Book Company, Inc., New York, 1950, p. 173-216.

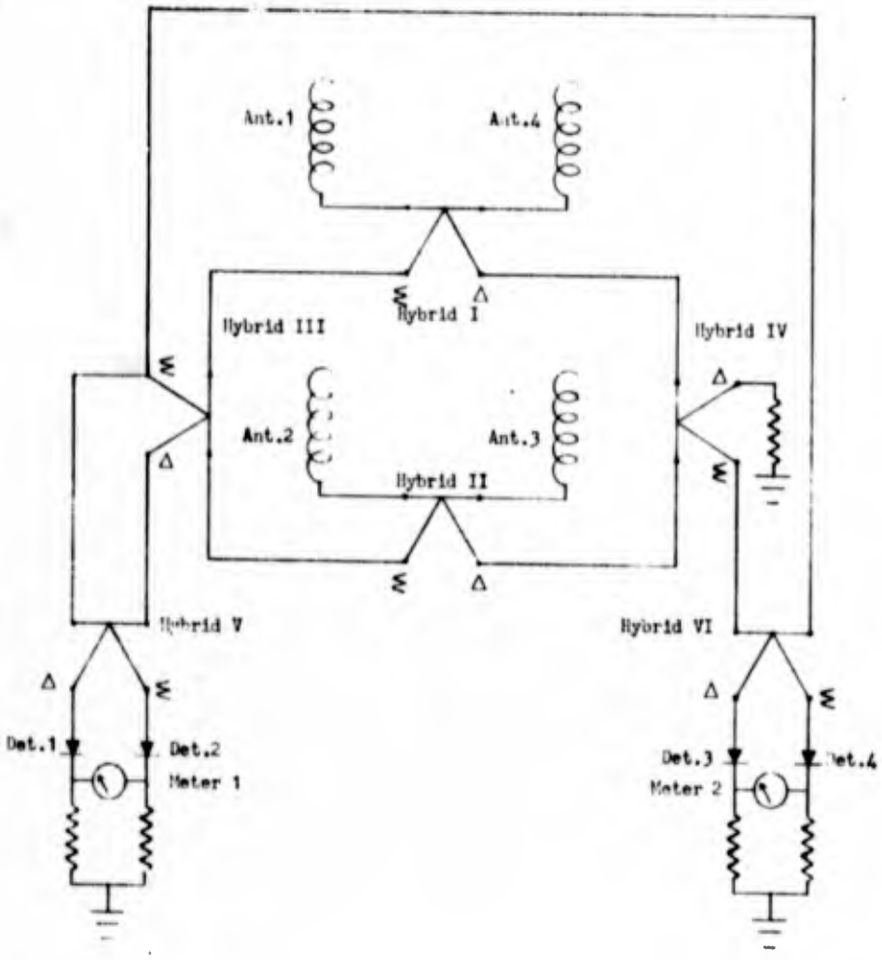

Figure 1. Circuit of four lobe monopulse system.

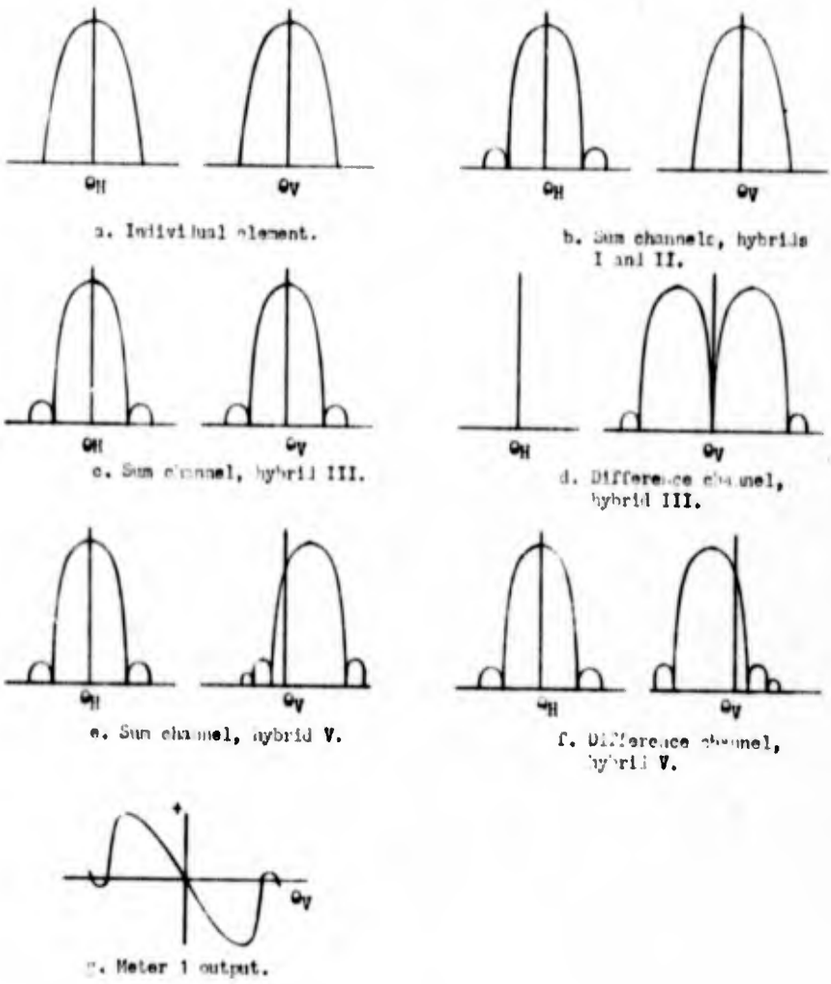

Figure 2. Development of monopulse radiation patterns.

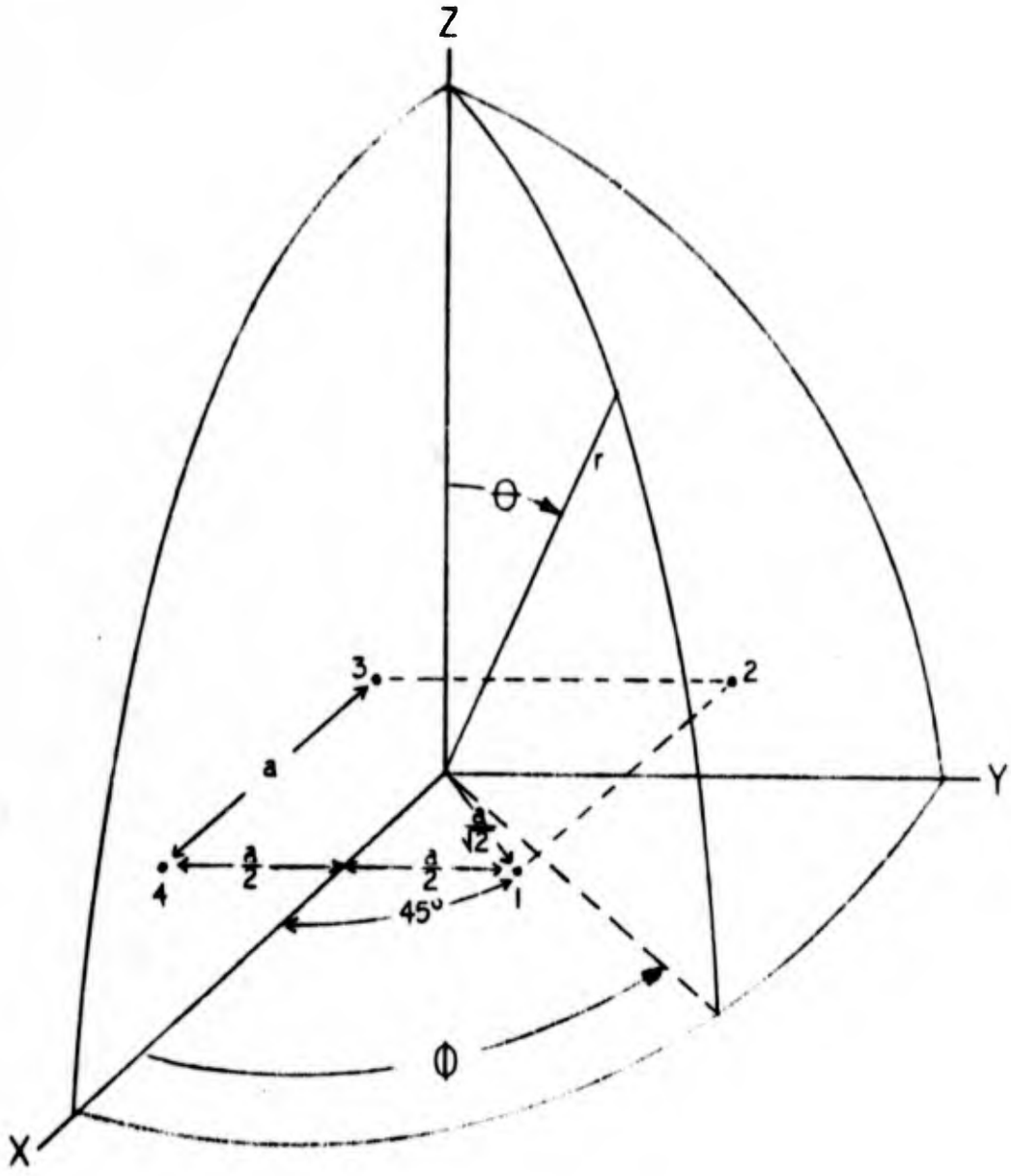

Figure 3. Geometry of an array of four sources.

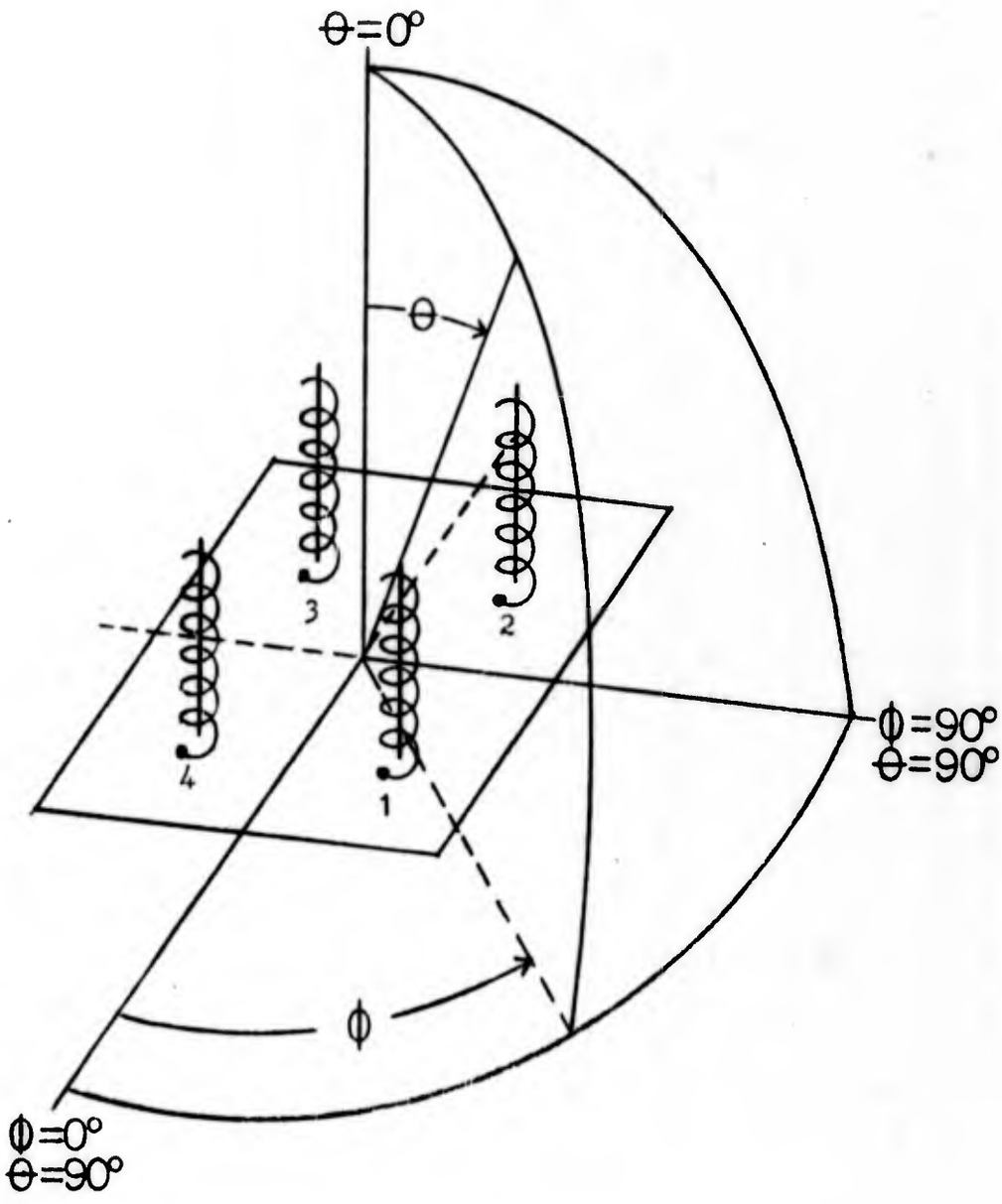

Figure 4. Coordinate system used in the measurements.

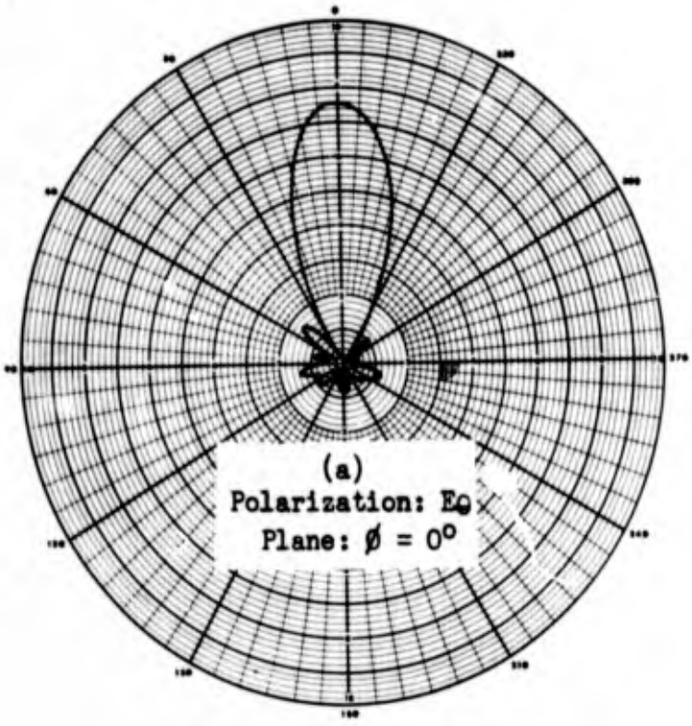

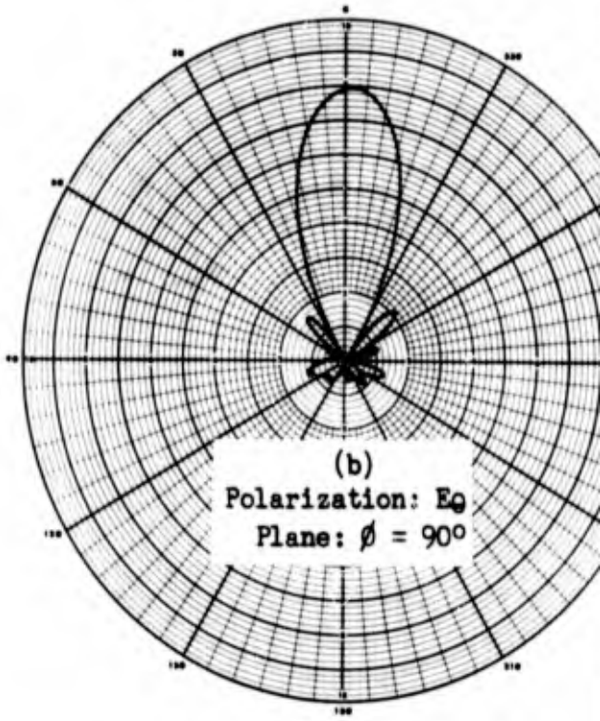

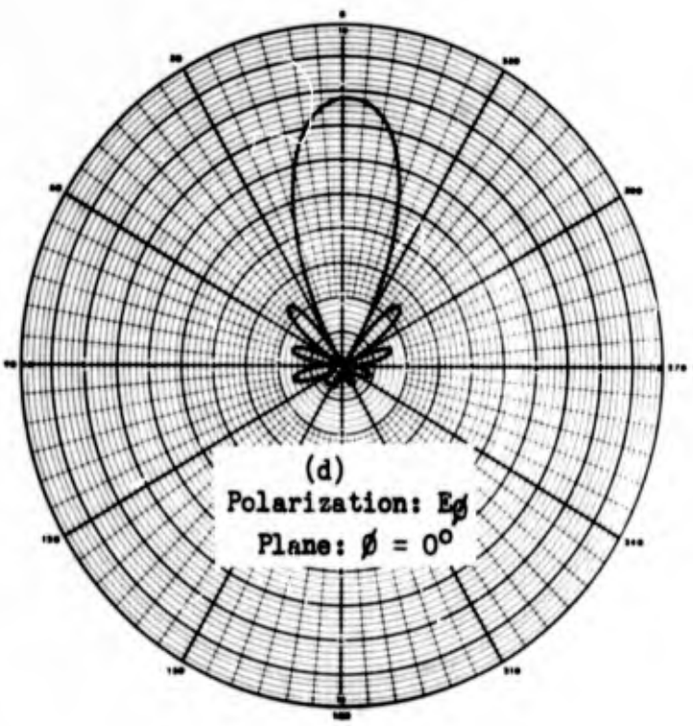

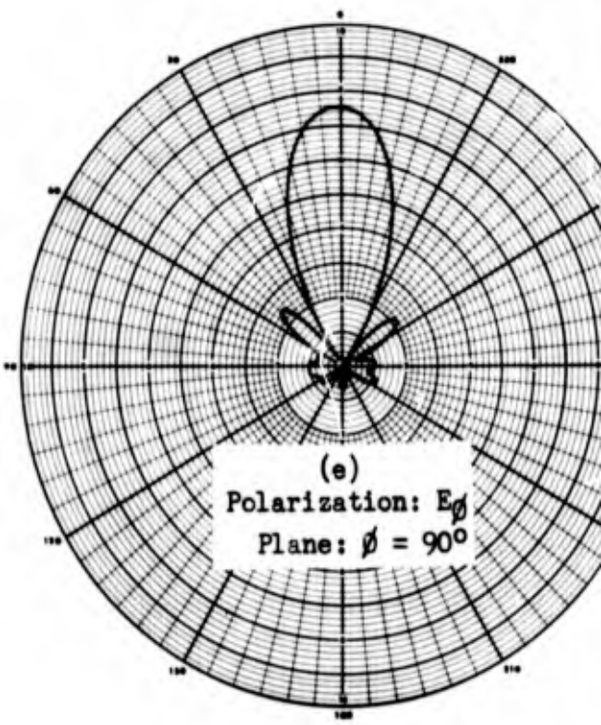

A

Figure 5. Radiation patterns of a single helix. Linear polarization, 1
Helix diameter = 2.88 inches, pitch = 12°, turns = 10, conduct

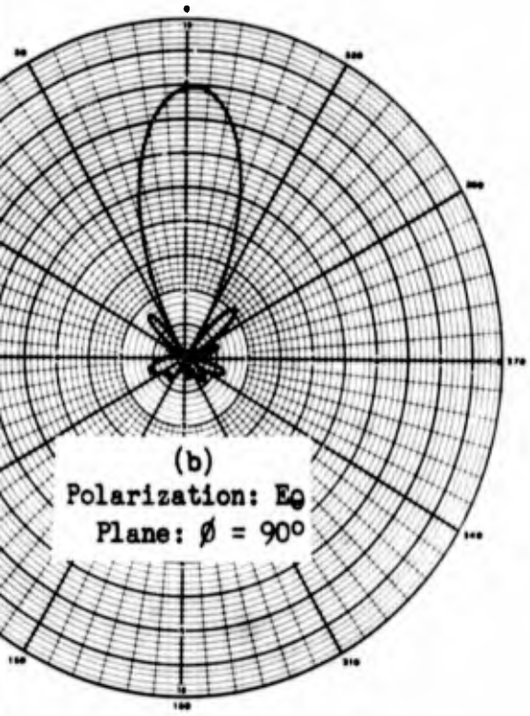

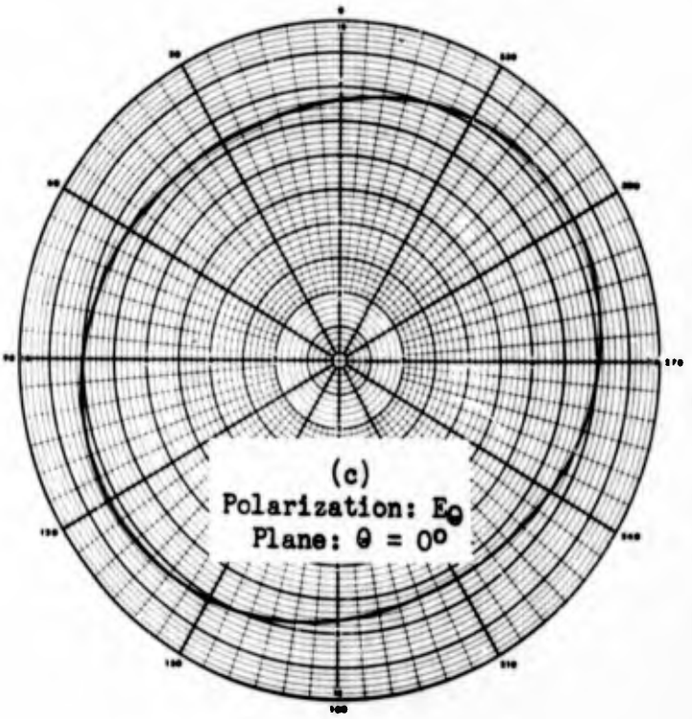

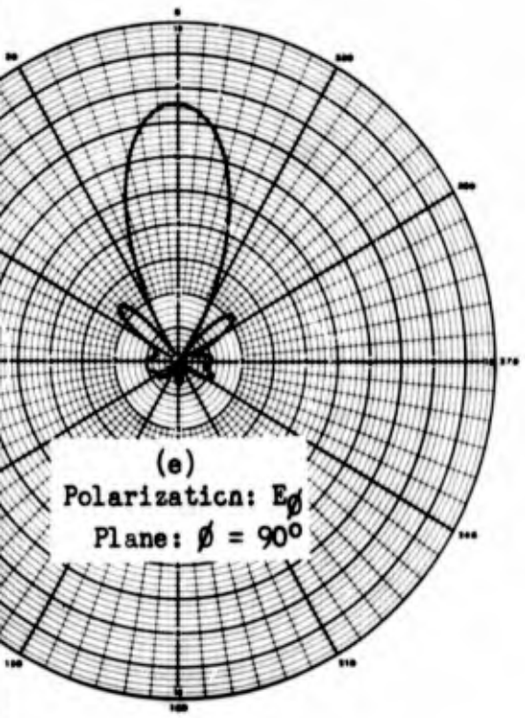

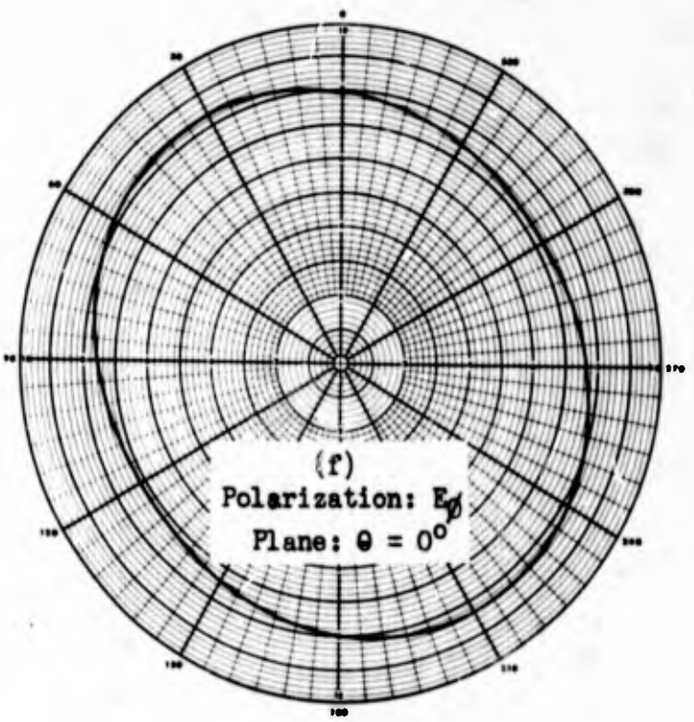

elix. Linear polarization, 1500 mcs.
tch = 12°, turns = 10, conductor diameter = 0.072 incnes.

B

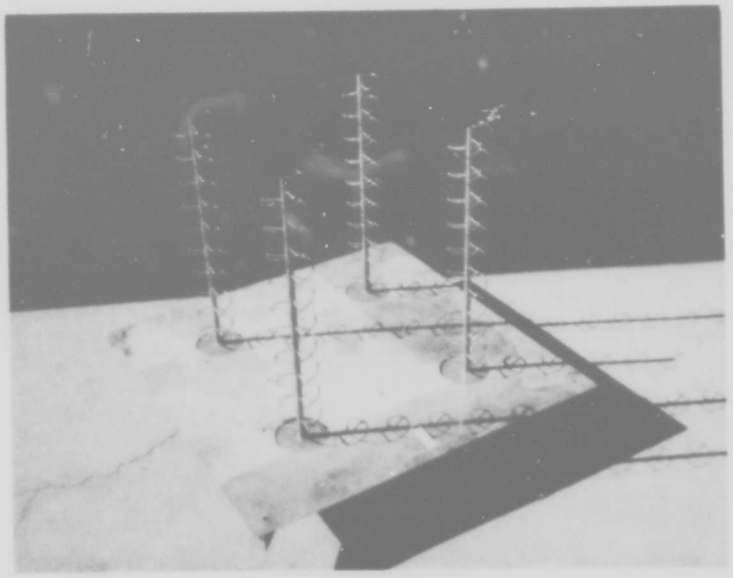

Figure 6. Four element helical array.

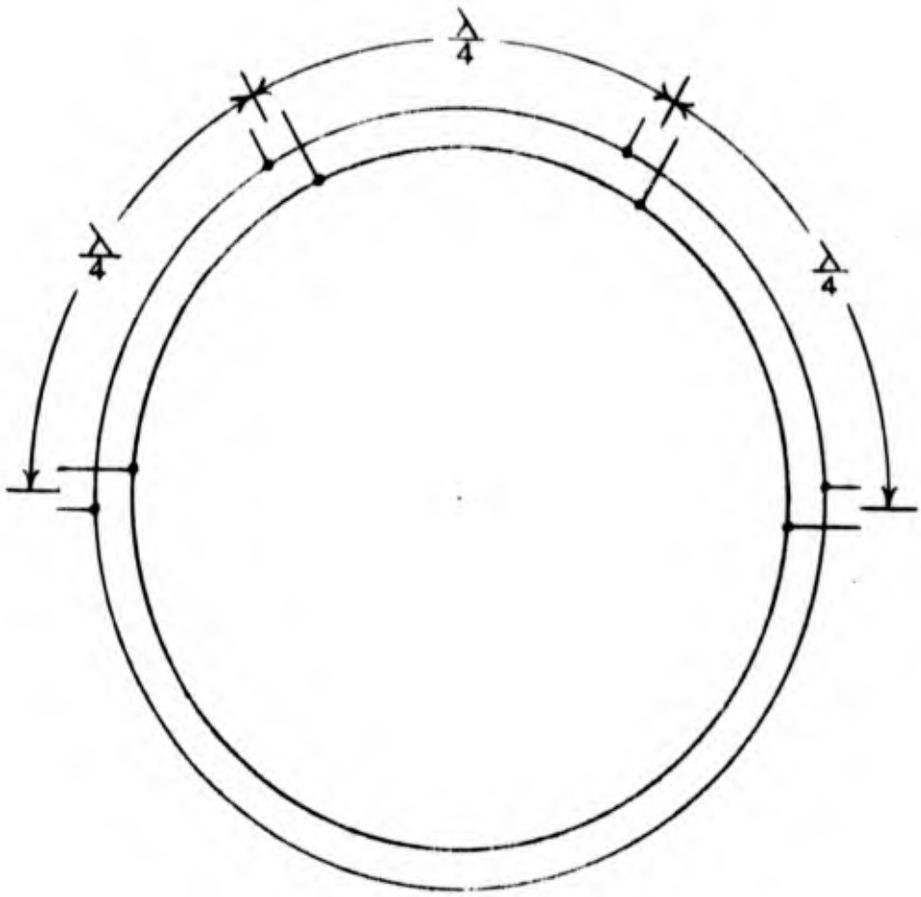

Figure 7. Electrical circuit of strip-line hybrids.

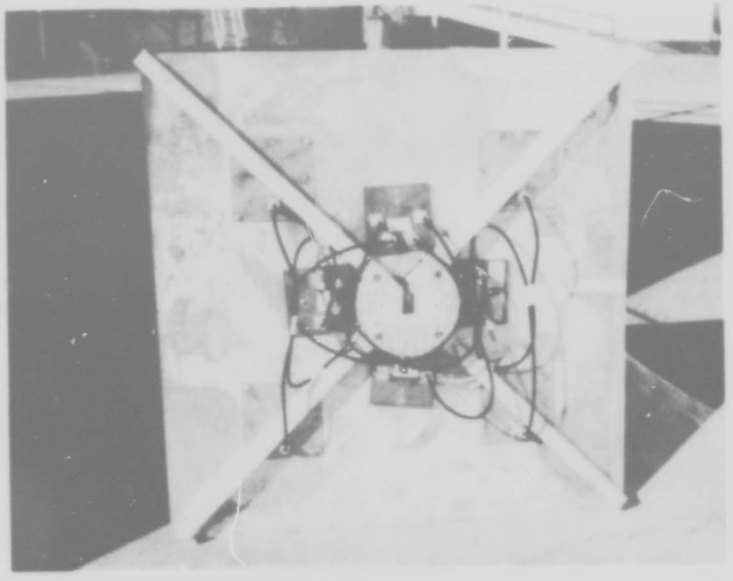

Figure 8. Photograph of hybrids mounted behind array ground plane.

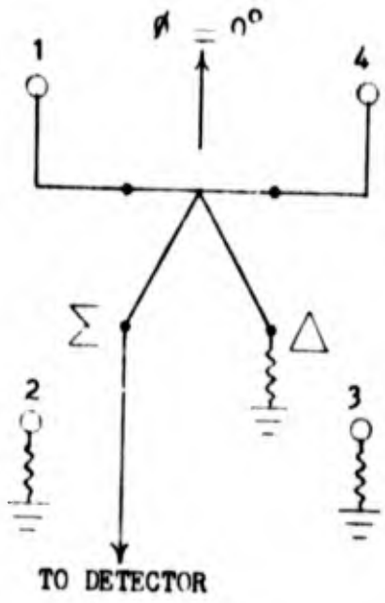

Figure 9. Circuit for sum of two adjacent elements.

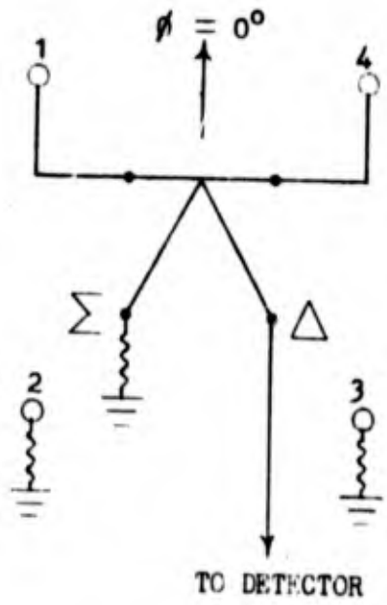

Figure 10. Circuit for difference of two adjacent elements.

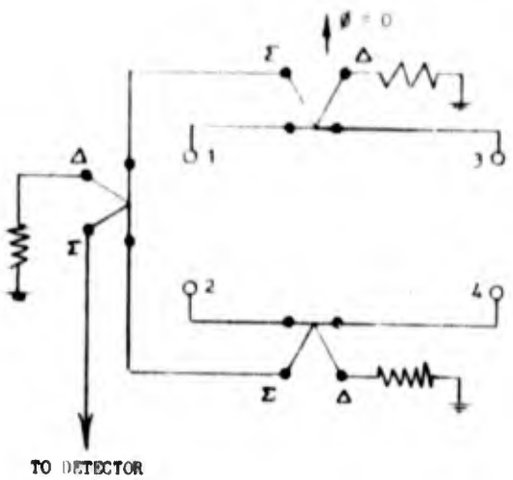

Figure 11. Circuit for sum of sums patterns of four element array.

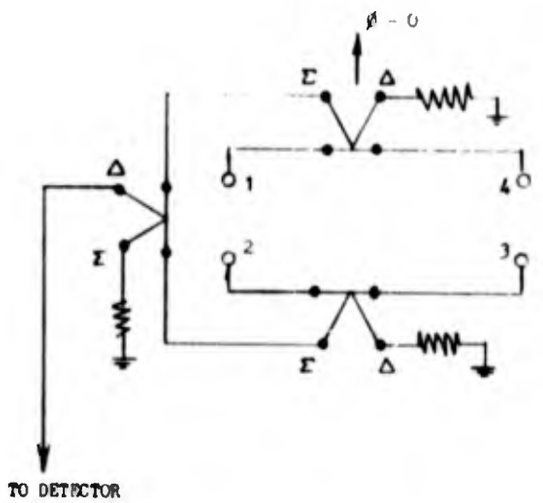

Figure 12. Circuit for difference of sums patterns of four element array.

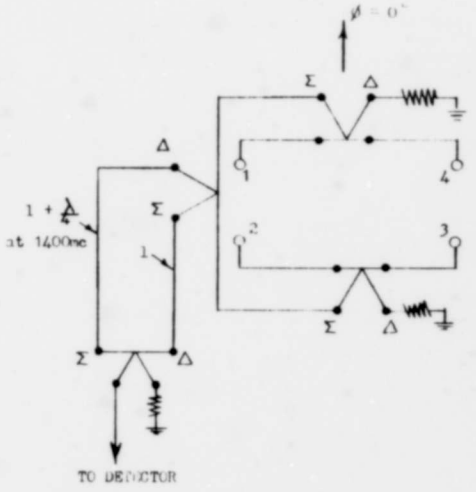

Figure 13. Circuit for sum of sum and difference patterns of four element array.

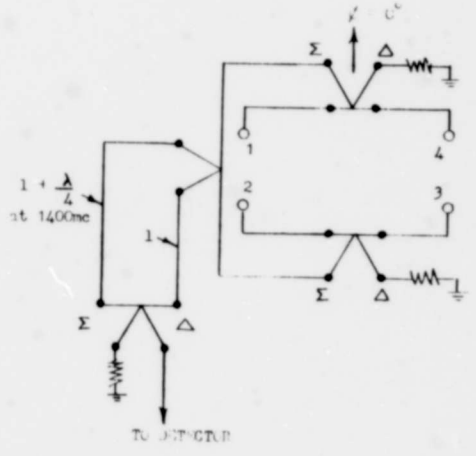

Figure 14. Circuit for difference of sum and difference patterns of four element array.

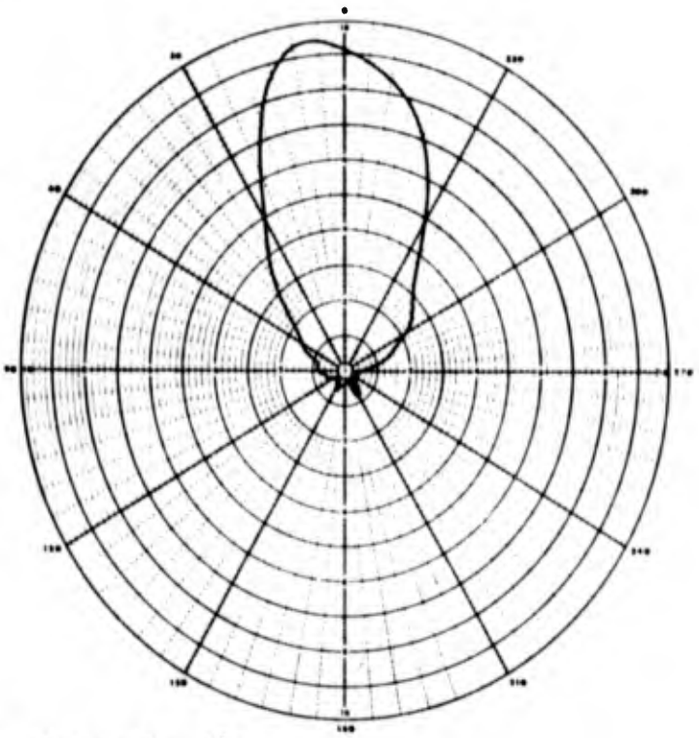

(a) Plane: $\phi = 0^{\circ}$

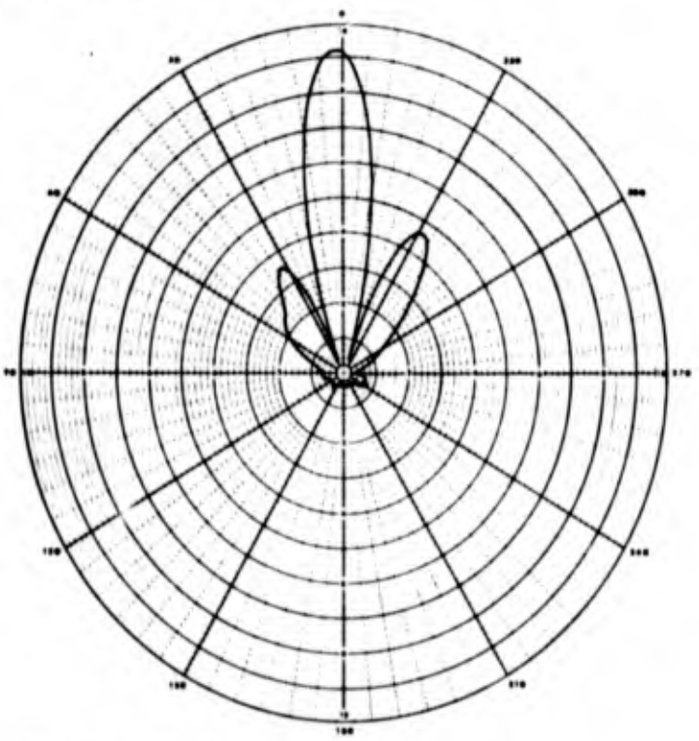

(b) Plane: $\phi = 90^{\circ}$

Figure 15. Sum patterns, two elements fed in phase through a hybrid. 1200 mc.

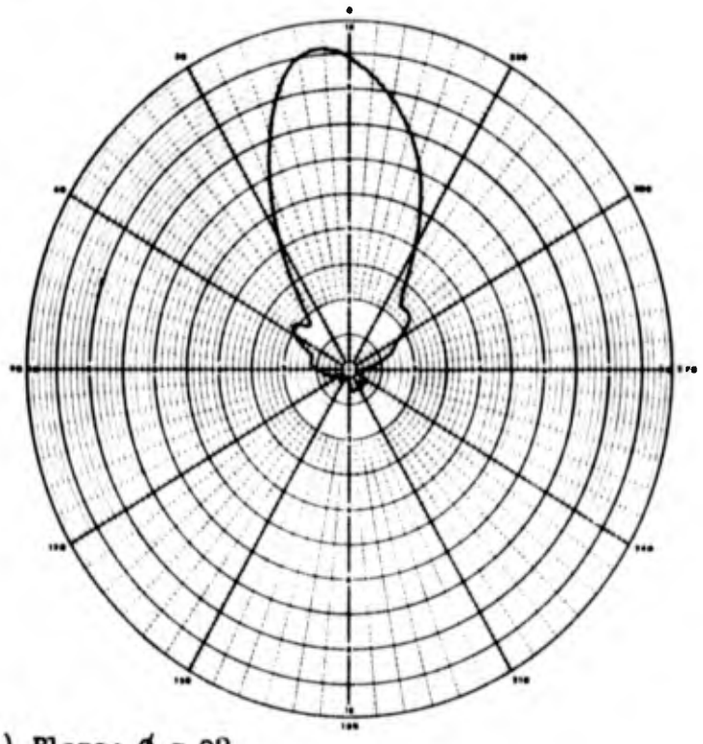

(a) Plane: $\phi = 0^{o}$

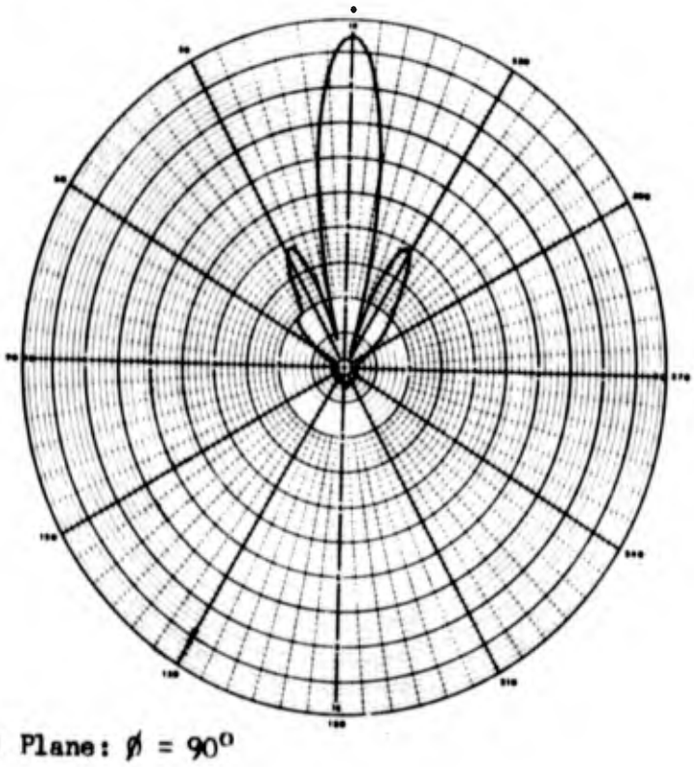

(b) Plane: $\phi = 90^{o}$

Figure 16: Sum patterns, two elements fed in phase through a hybrid. 1300 mc.

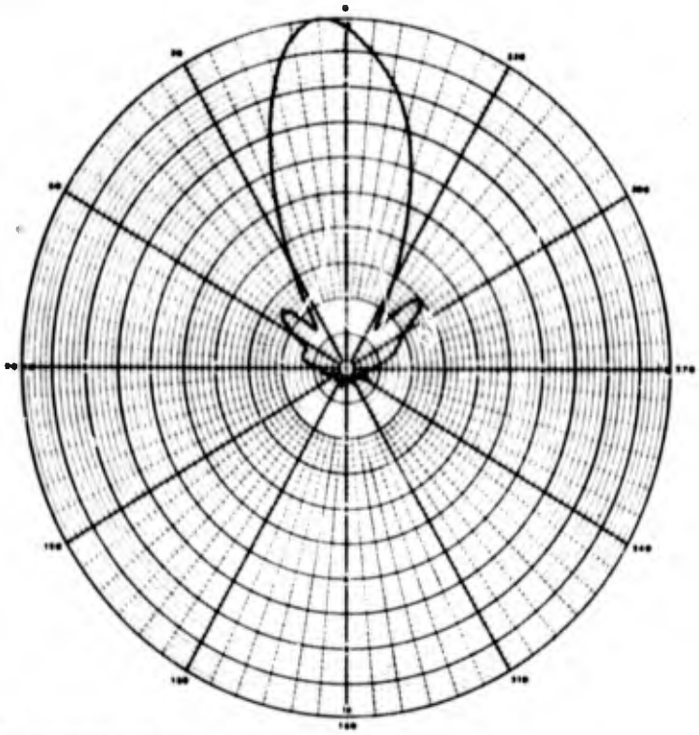

(a) Plane: $\phi = 0^{o}$

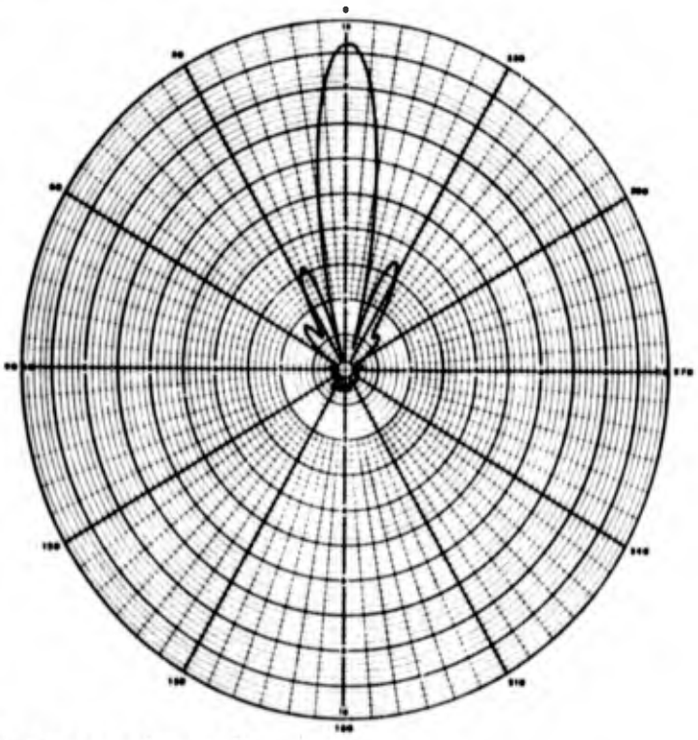

(b) Plane: $\phi = 90^{o}$

Figure 17: Sum patterns, two elements fed in phase through a hybrid. 1400 mc/s

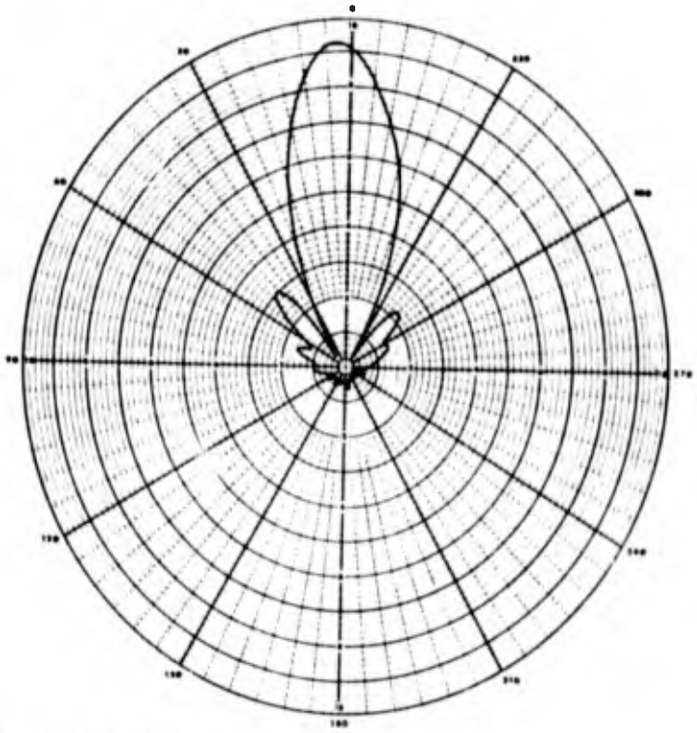

(a) Plane: $\phi = 0^{\circ}$

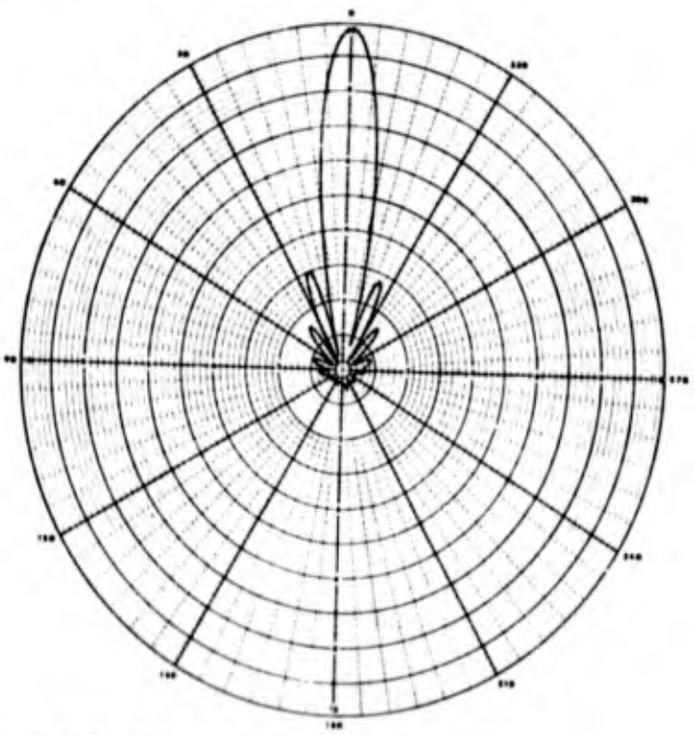

(b) Plane: $\phi = 90^{\circ}$

Figure 18: Sum patterns, two elements fed in phase through a hybrid. 1500 mc.

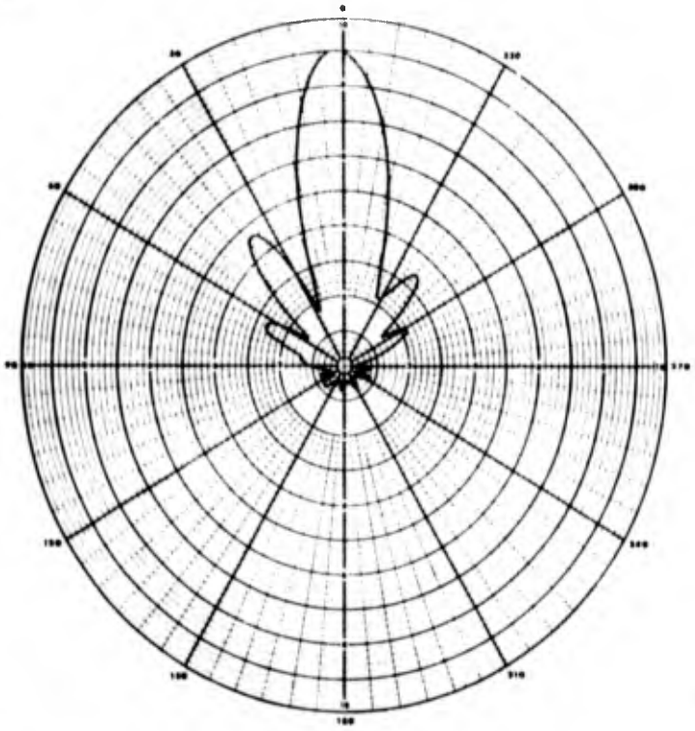

(a) Plane: $\phi = 0^{o}$

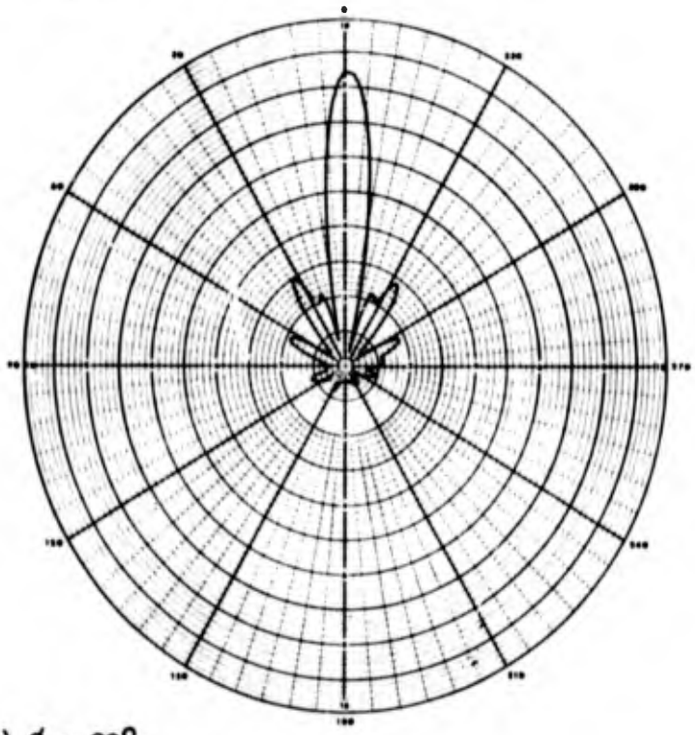

(b) $\phi = 90^{o}$

Figure 19. Sum patterns, two elements fed in phase through a hybrid. 1600 mc.

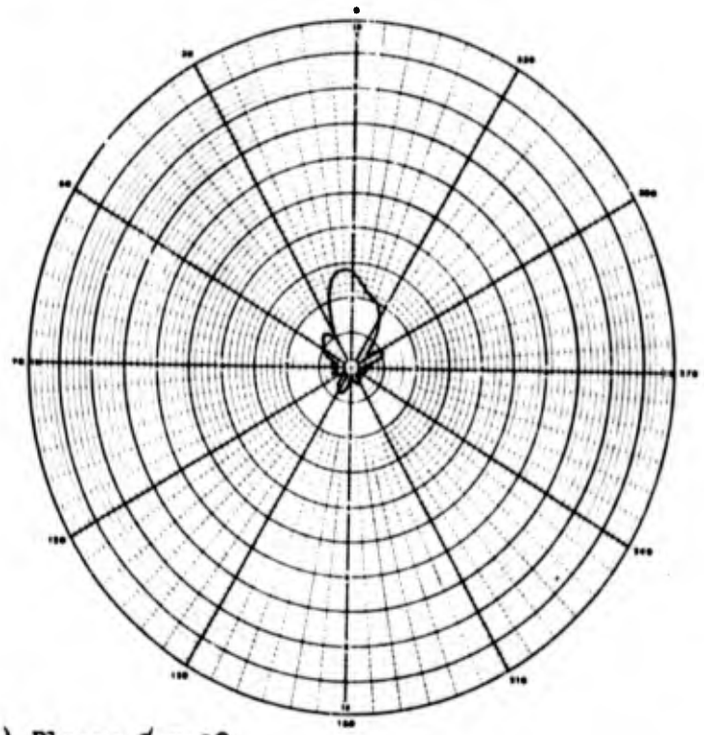

(a) Plane: $\phi = 0^{\circ}$

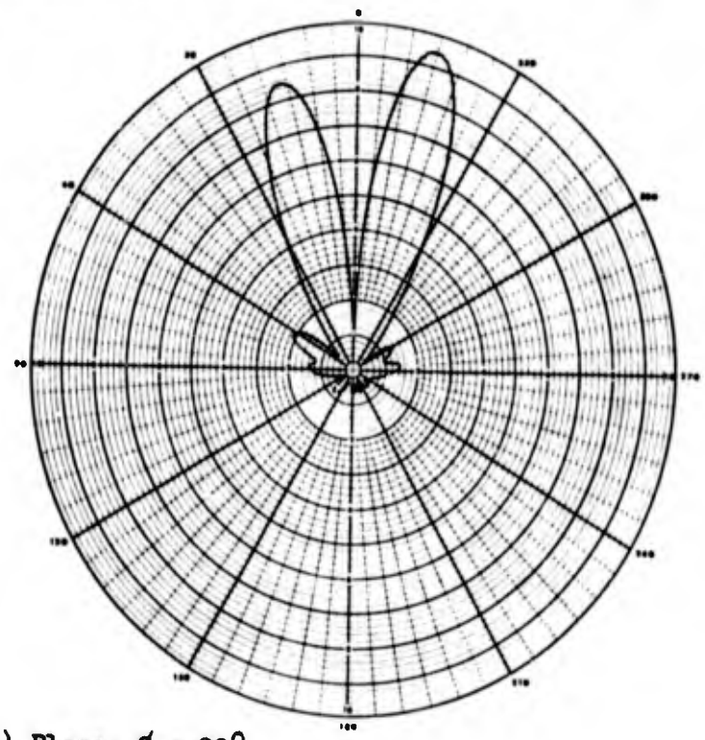

(b) Plane: $\phi = 90^{\circ}$

Figure 20. Difference patterns, two elements fed 180° in phase through a hybrid. 1200 mc.

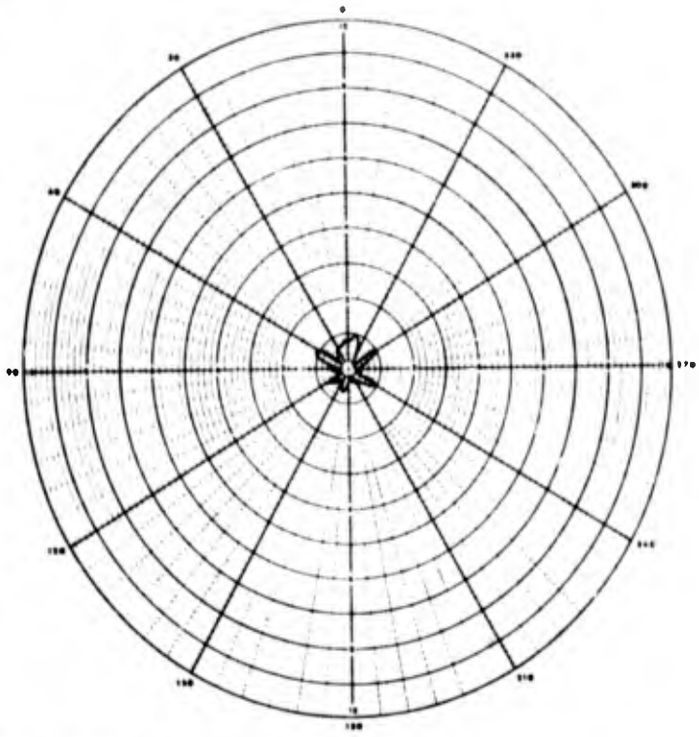

(a) Plane: $\phi = 0^{\circ}$

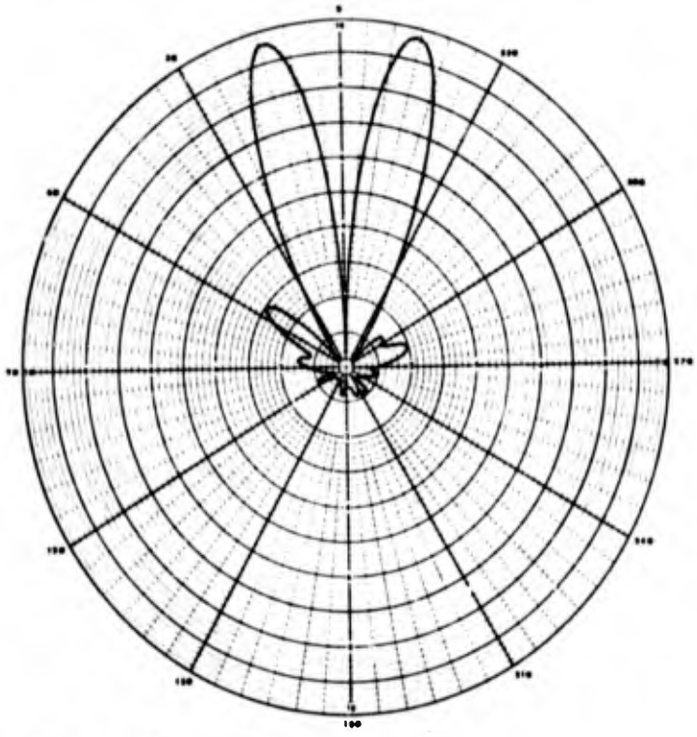

(b) Plane: $\phi = 90^{\circ}$

Figure 21. Difference patterns, two elements fed 180° in phase through a hybrid. 1300 mc.

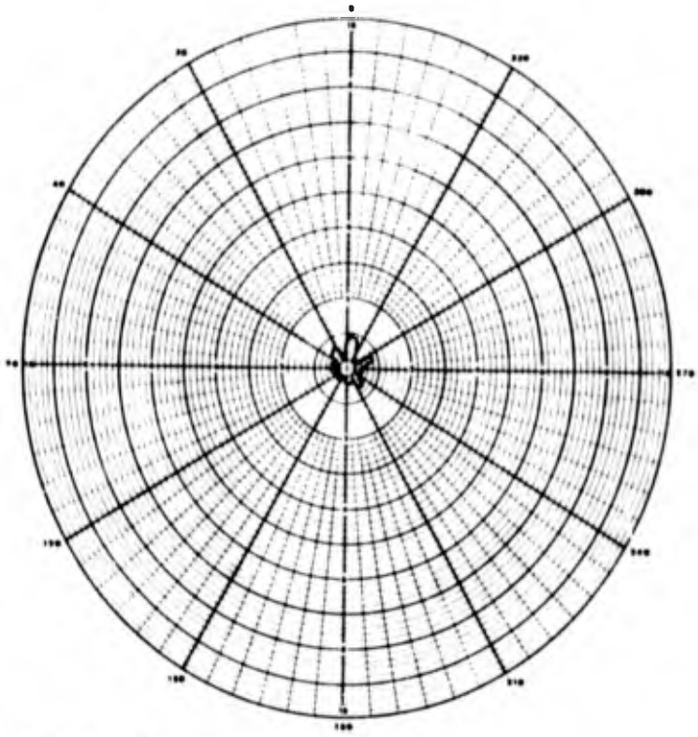

(a) Plane: $\phi = 0^{o}$

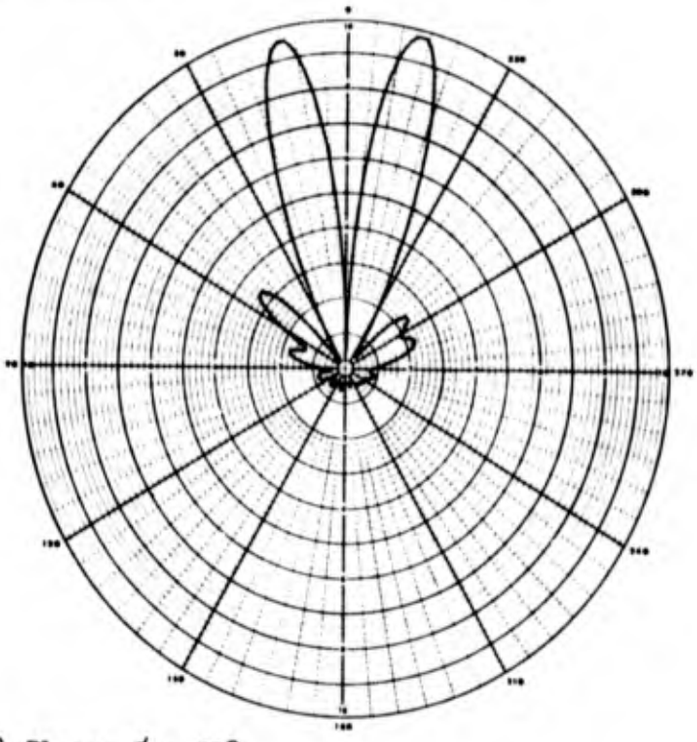

(b) Plane: $\phi = 90^{o}$

Figure 22. Difference patterns, two elements fed 180° in phase through a hybrid. 1400 mc.

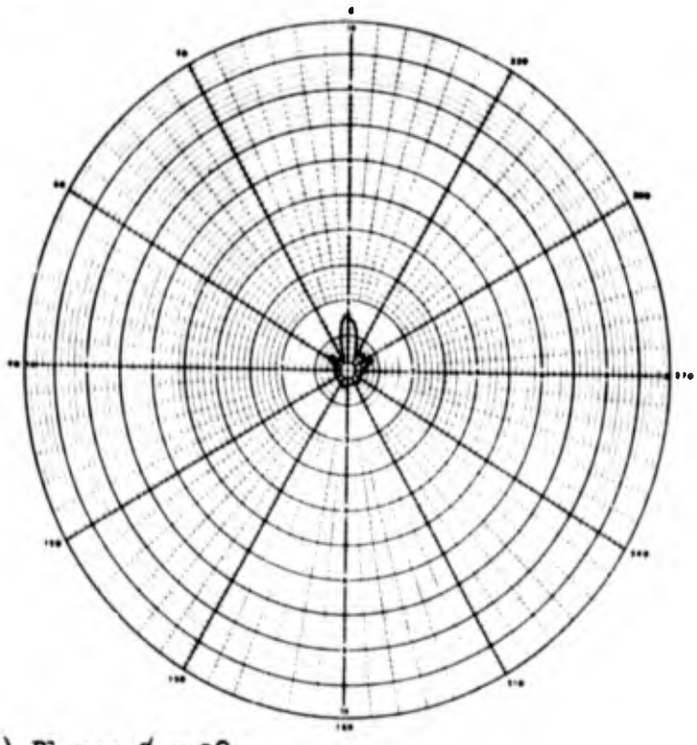

(a) Plane: $\phi = 0^{\circ}$

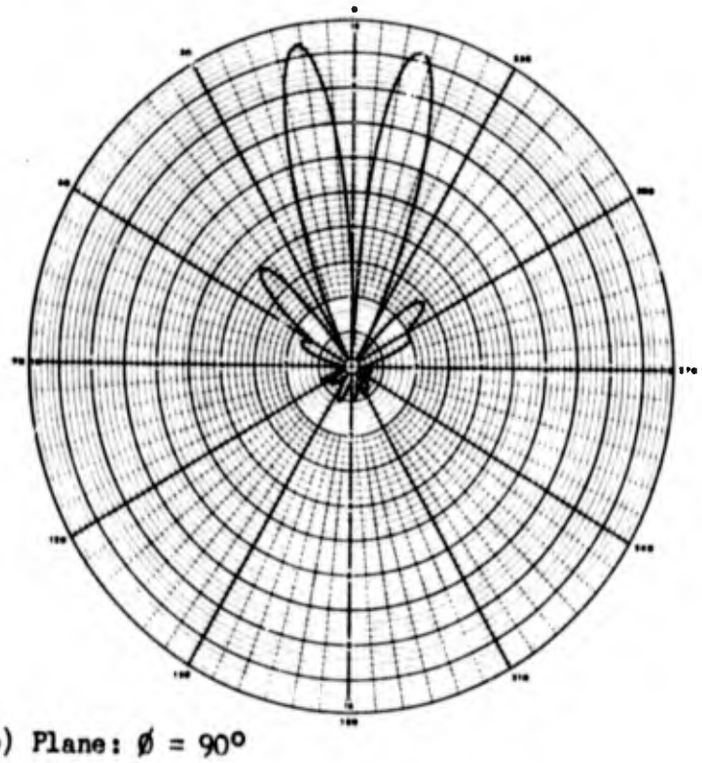

(b) Plane: $\phi = 90^{\circ}$

Figure 23. Difference patterns, two elements fed 180° in phase through a hybrid. 1500 mc.

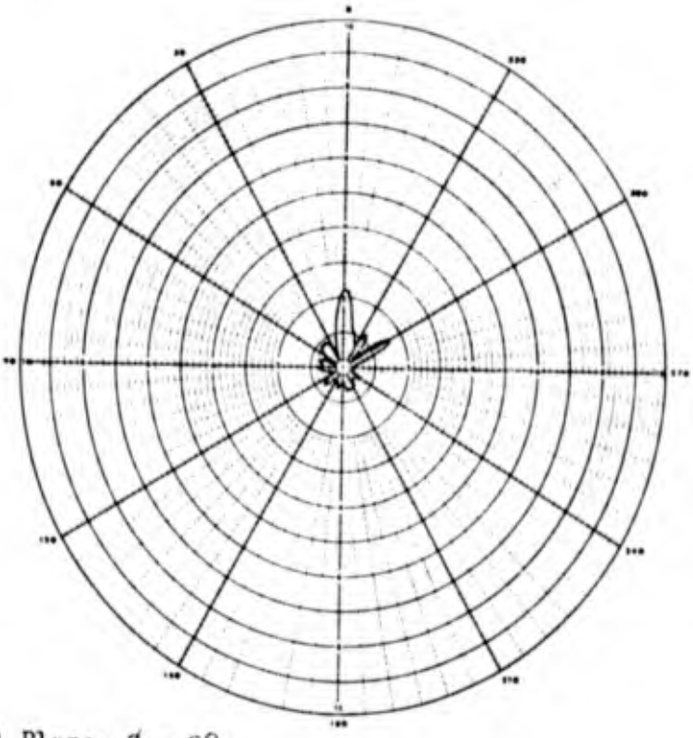

(a) Plane: $\phi = 0^{o}$

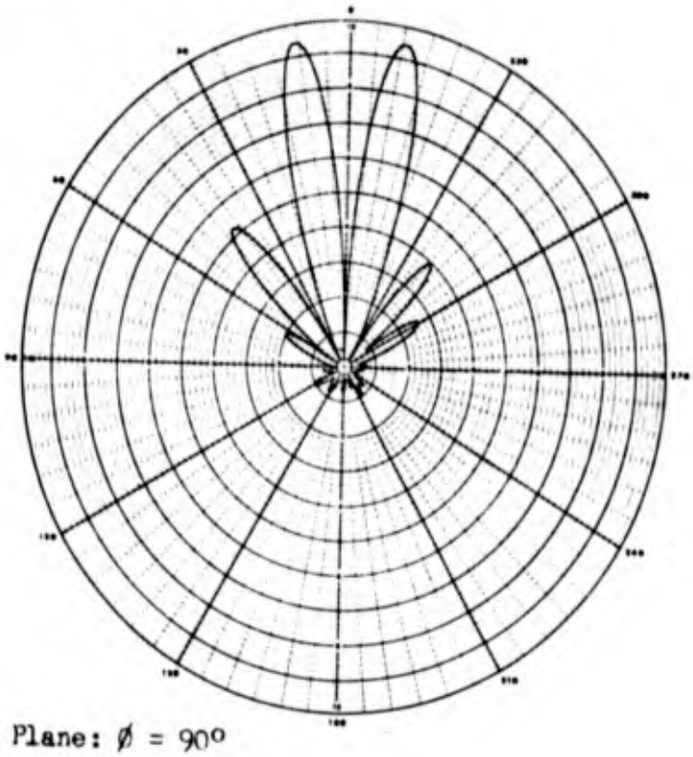

(b) Plane: $\phi = 90^{o}$

Figure 24. Difference patterns, two elements fed 180° in phase through a hybrid. 1600 mc.

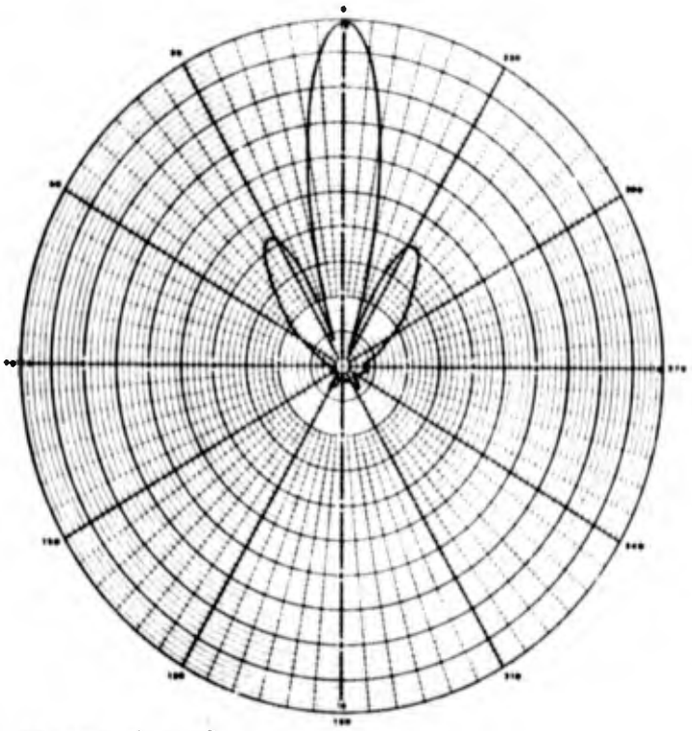

(a) Plane: $\phi = 0^{o}$

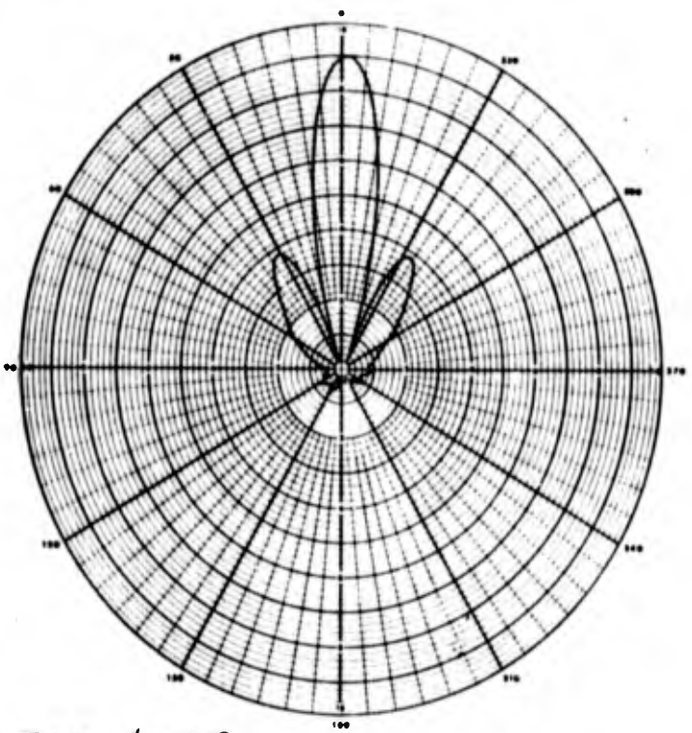

(b) Plane: $\phi = 90^{o}$

Figure 25. Sum of the sums patterns, four elements fed in phase through hybrids. 1200 mc.

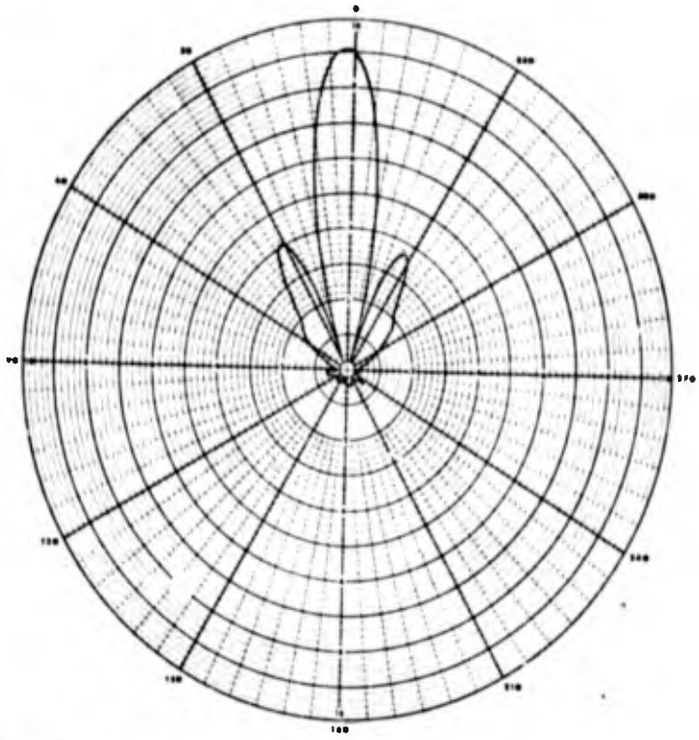

(a) Plane: $\phi = 0^{\circ}$

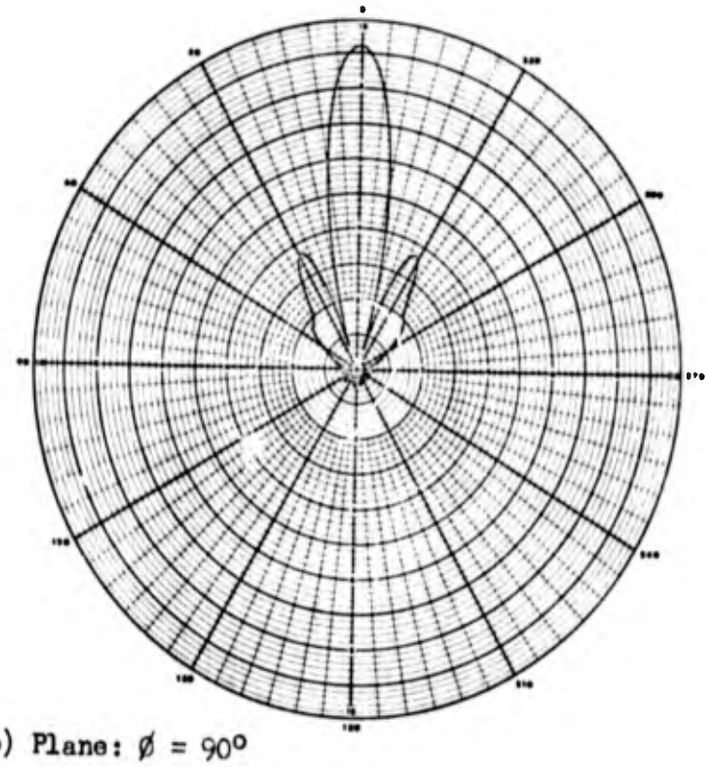

(b) Plane: $\phi = 90^{\circ}$

Figure 26. Sum of the sums patterns, four elements fed in phase through hybrids. 1300 mc.

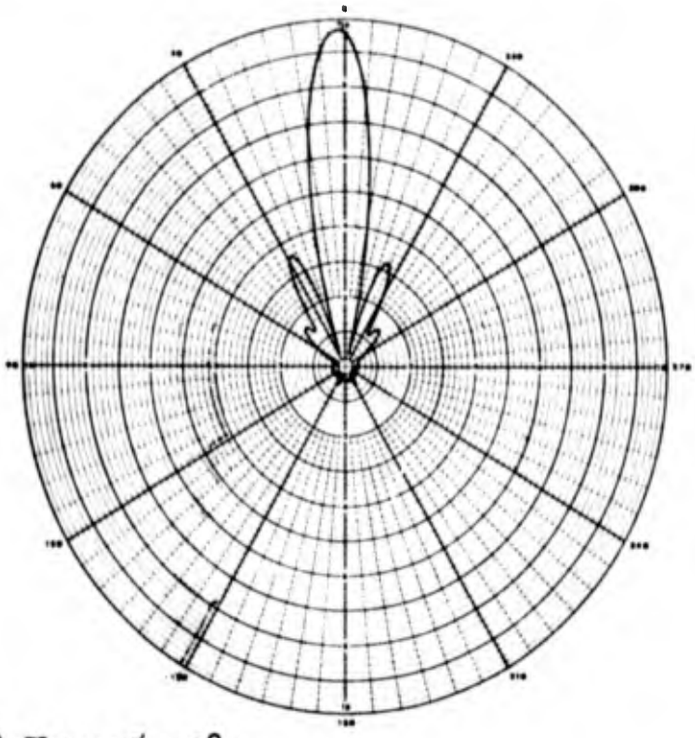

(a) Plane: $\phi = 0^{\circ}$

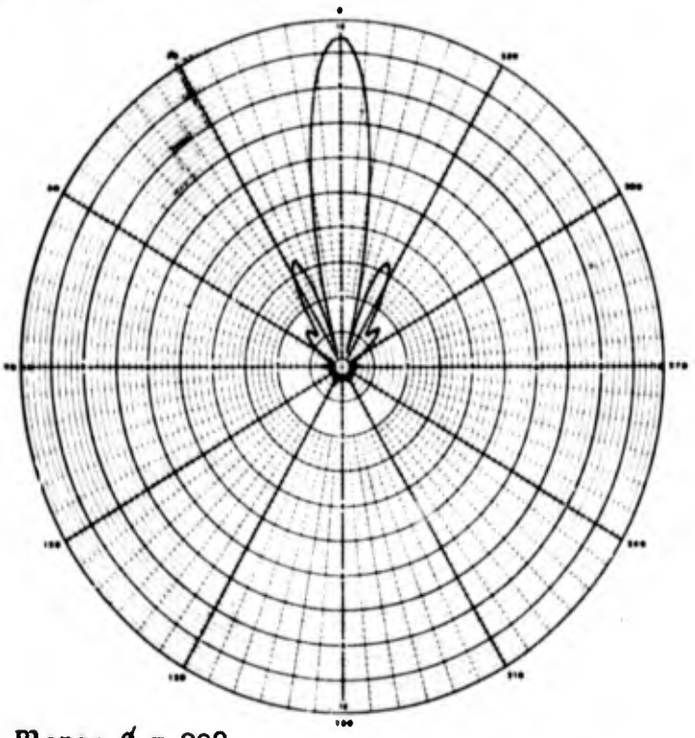

(b) Plane: $\phi = 90^{\circ}$

Figure 27. Sum of the sums patterns, four elements fed in phase through hybrids. 1400 mc.

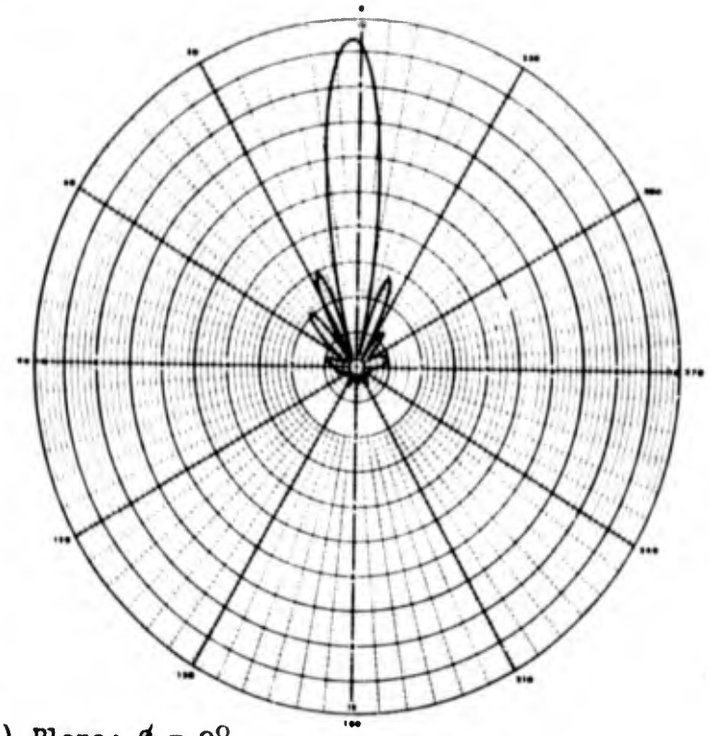

(a) Plane: ϕ = 0°

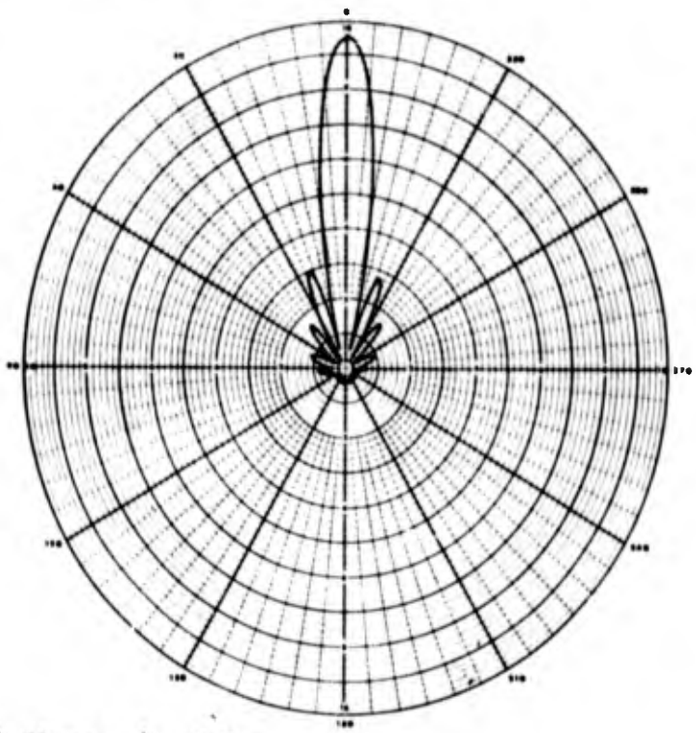

(b) Plane: ϕ = 90°

Figure 28. Sum of the sums patterns, four elements fed in phase through hybrids. 1500 mc.

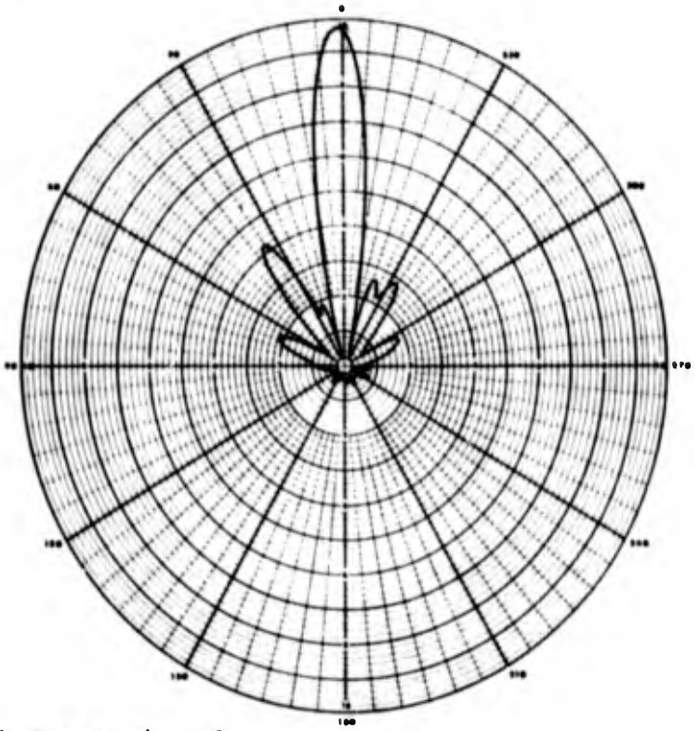

(a) Plane: $\phi = 0^{o}$

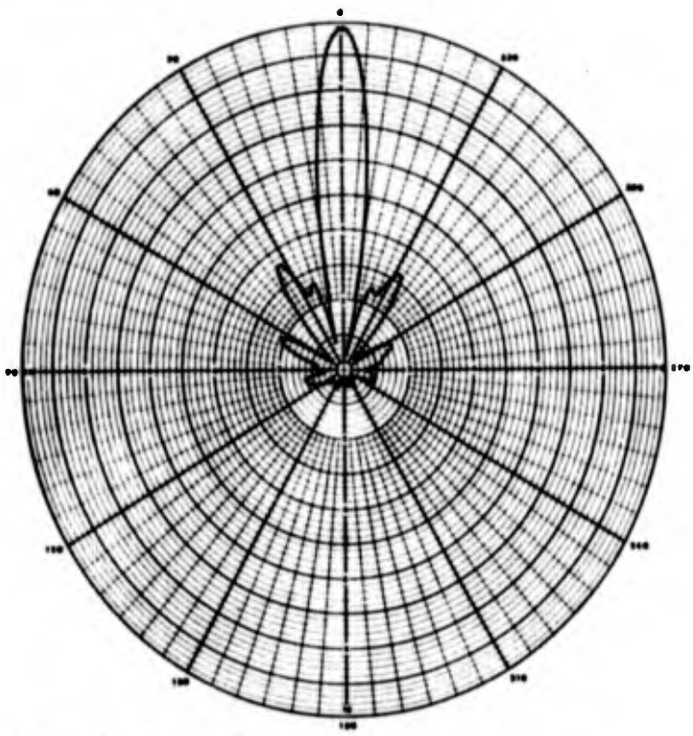

(b) Plane: $\phi = 90^{o}$

Figure 29. Sum of the sums patterns, four elements fed in phase through hybrids. 1600 mc.

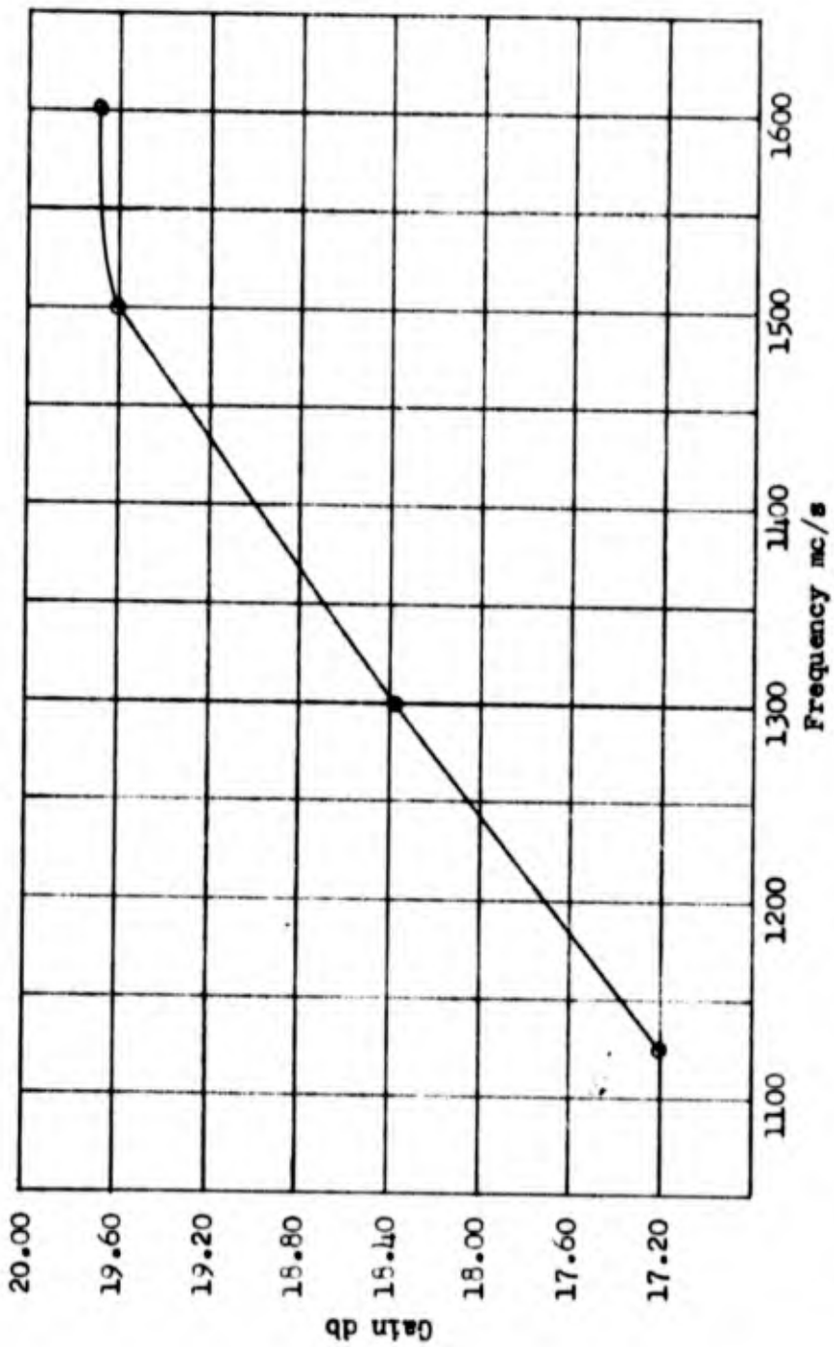

Figure 30. Gain of four element helical array, all elements fed in phase.

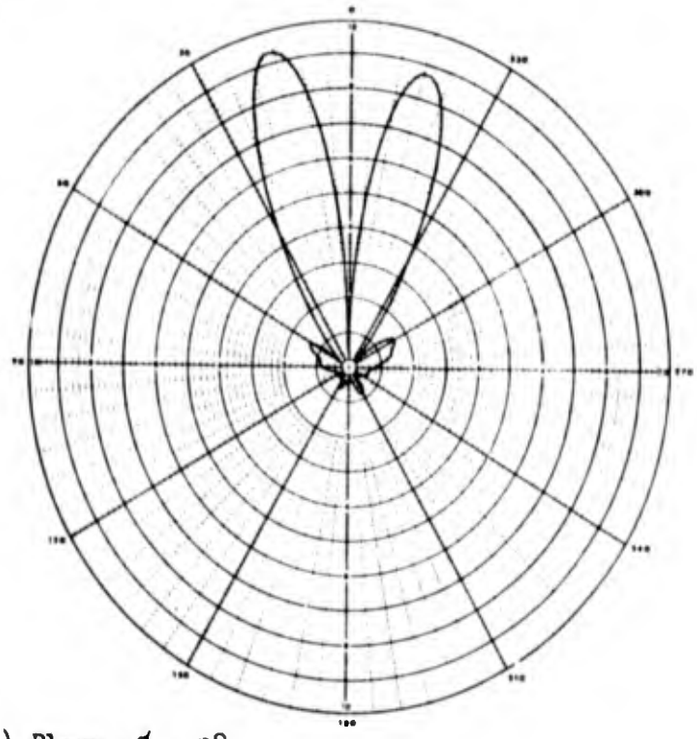

(a) Plane: $\phi = 0^{\circ}$

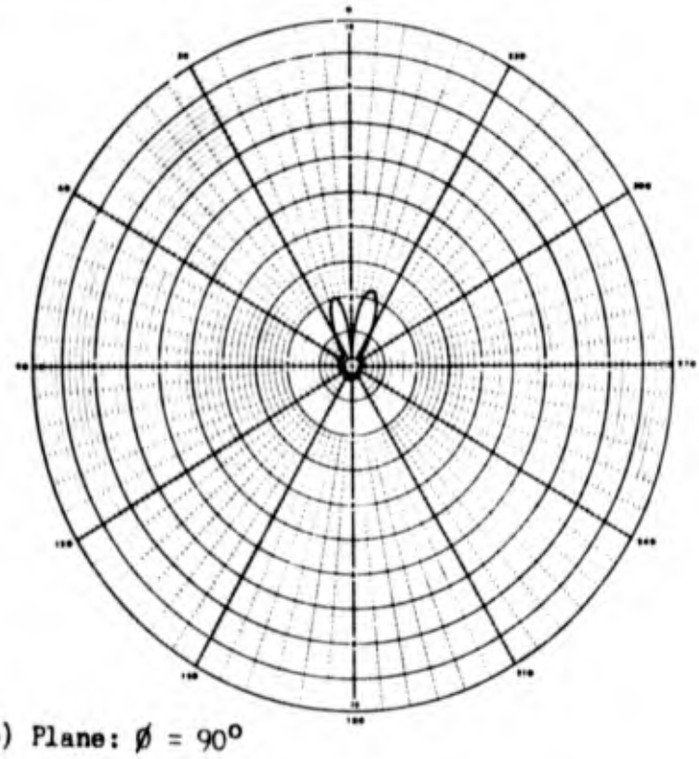

(b) Plane: $\phi = 90^{\circ}$

Figure 31. Difference of the sums patterns, two pairs of adjacent elements fed in phase, with pairs of elements fed 180° in phase. 1200 mc.

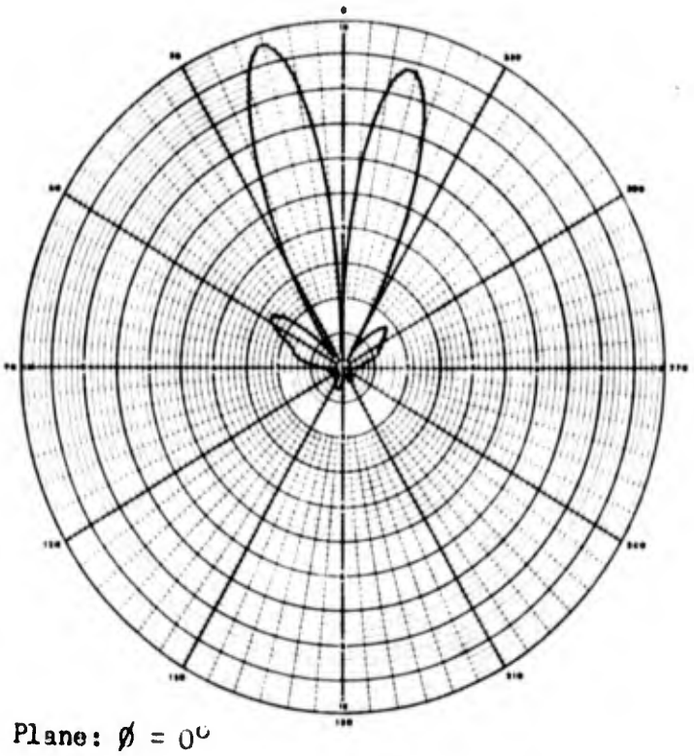

(a) Plane: $\phi = 0^{\circ}$

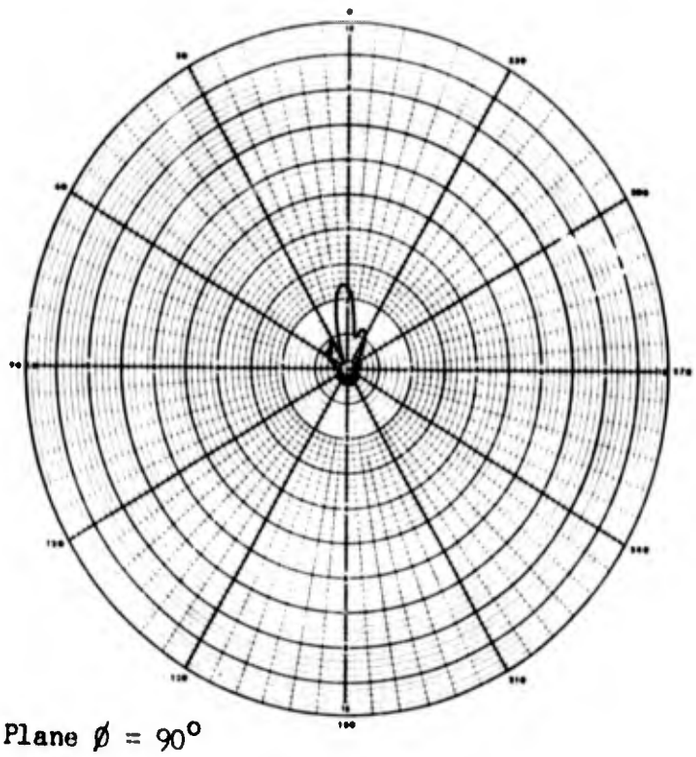

(b) Plane $\phi = 90^{\circ}$

Figure 32. Difference of the sums patterns, two pairs of adjacent elements fed in phase, with pairs of elements fed 180° in phase. 1300 mc.

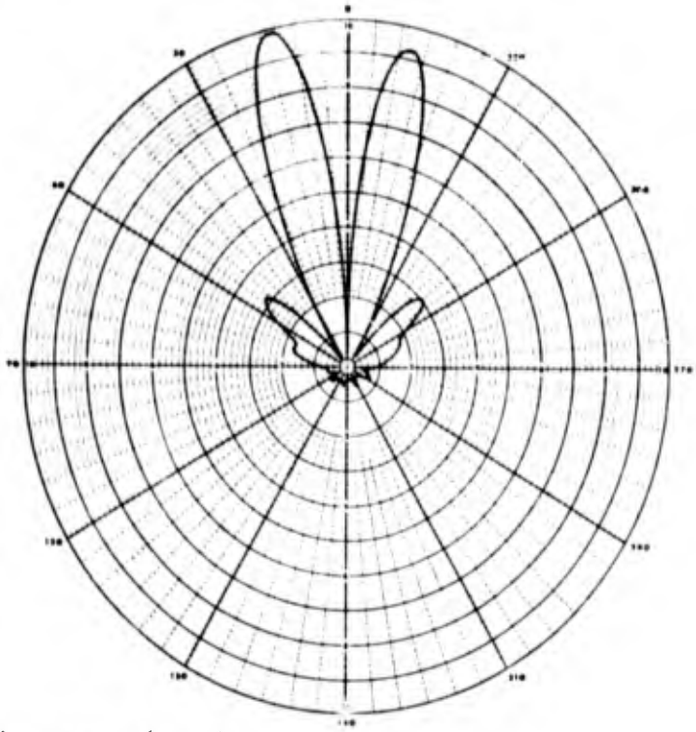

(a) Plane: $\phi = 0^{\circ}$

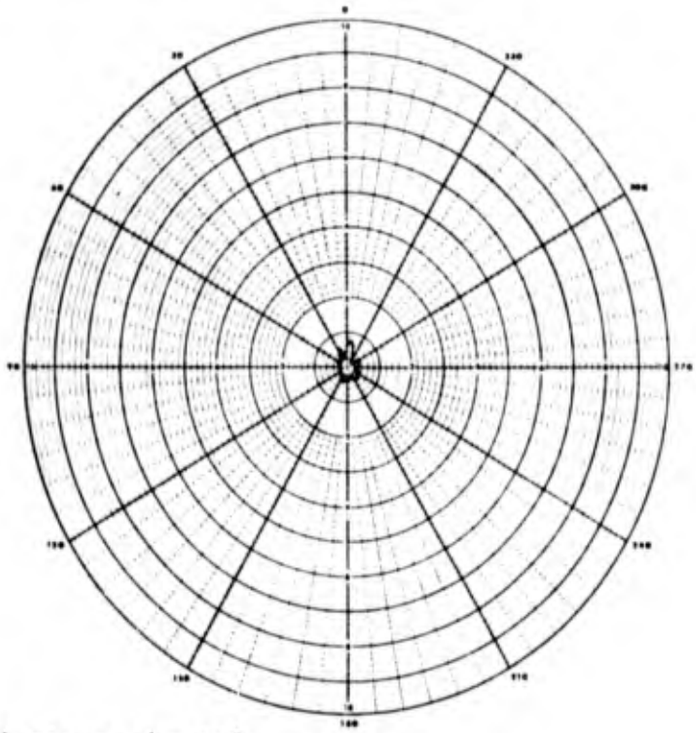

(b) Plane: $\phi = 90^{\circ}$

Figure 33. Difference of the sums patterns, two pairs of adjacent elements fed in phase, with pairs of elements fed 180° in phase. 1400 mc.

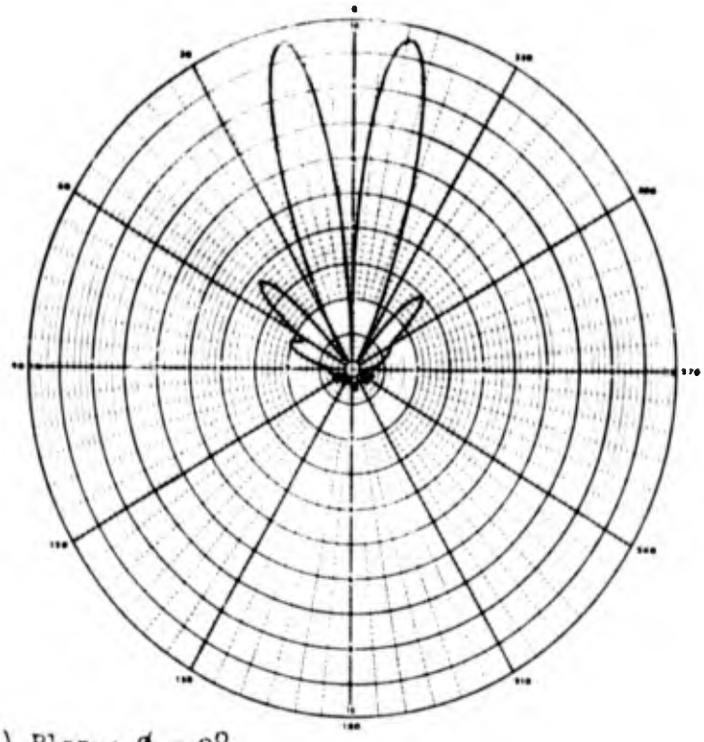

(a) Plane: $\phi = 0^\circ$

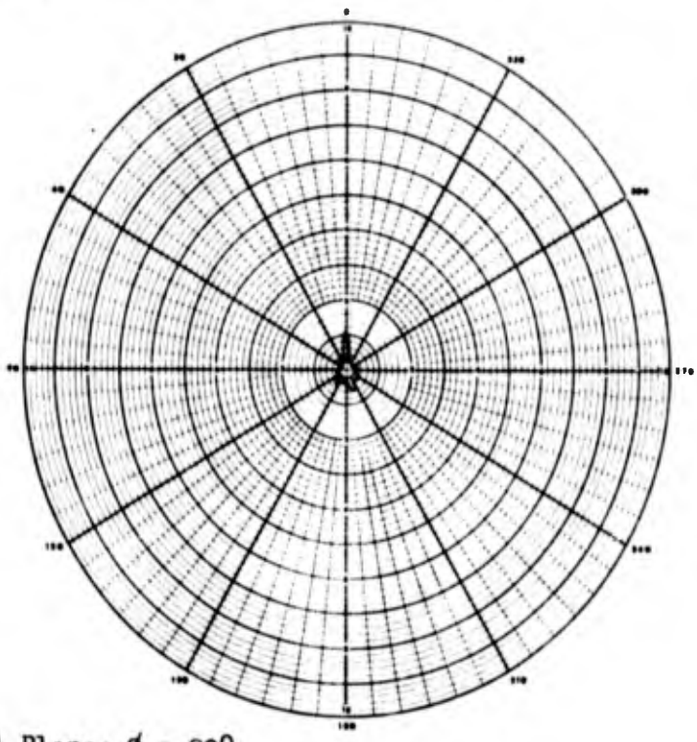

(b) Plane: $\phi = 90^\circ$

Figure 34. Difference of the sums patterns, two pairs of adjacent elements fed in phase, with pairs of elements fed 180° in phase. 1500 mc.

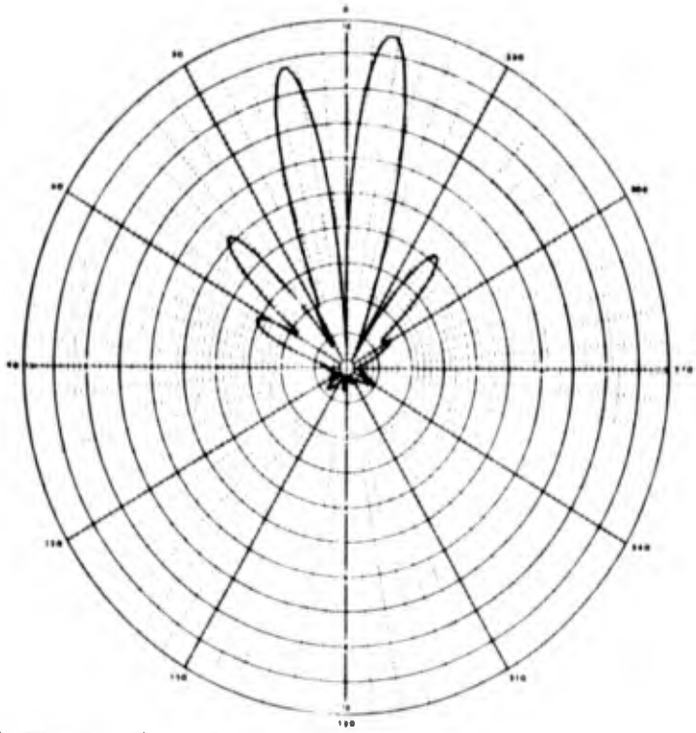

(a) Plane: $\phi = 0^{o}$

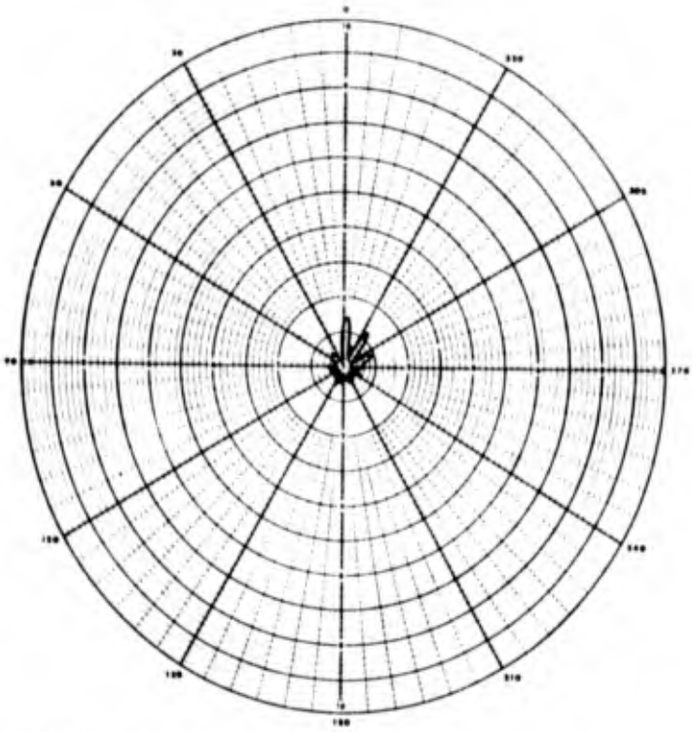

(b) Plane: $\phi = 90^{o}$

Figure 35. Difference of the sums patterns, two pairs of adjacent elements fed in phase, with pairs of elements fed 180° in phase. 1600 mc.

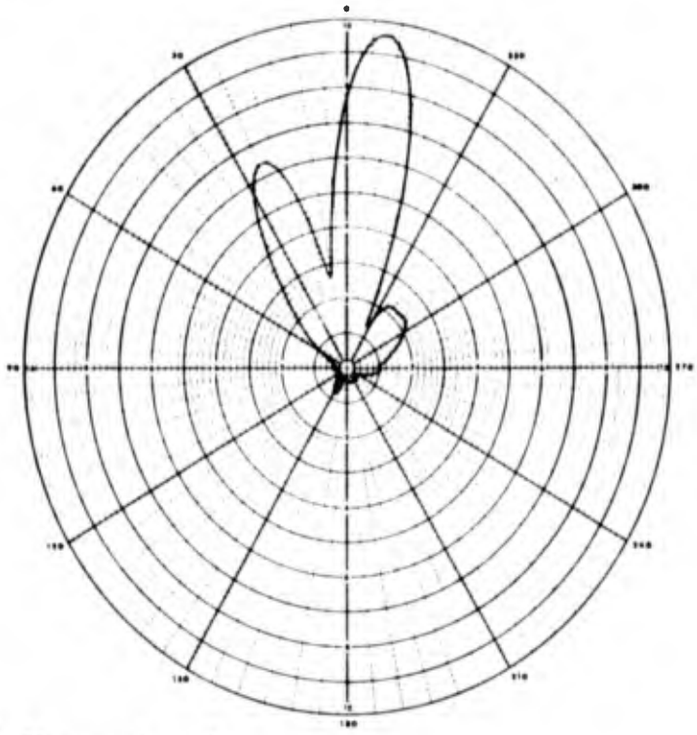

(a) Plane: $\phi = 0^{o}$

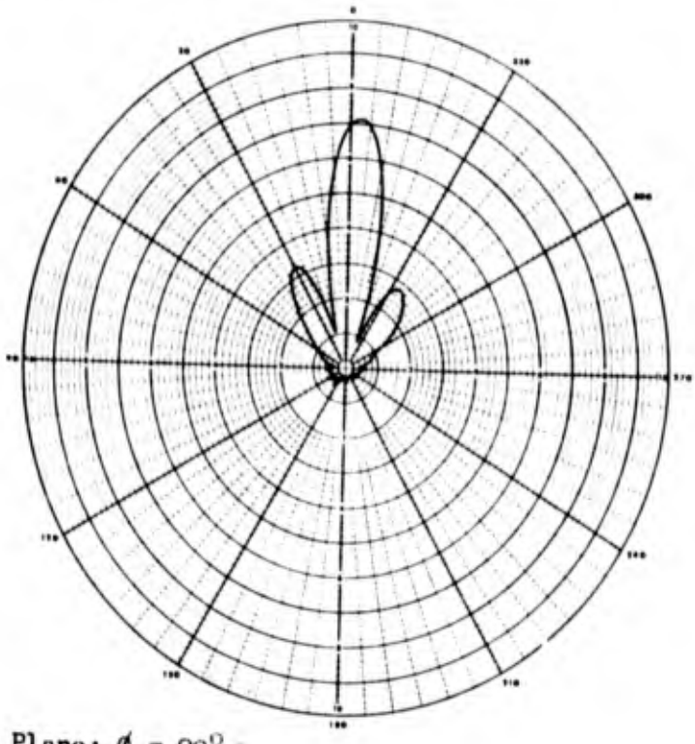

(b) Plane: $\phi = 90^{o}$

Figure 36. Sum of sum and difference patterns of four element array. 1200 mc.

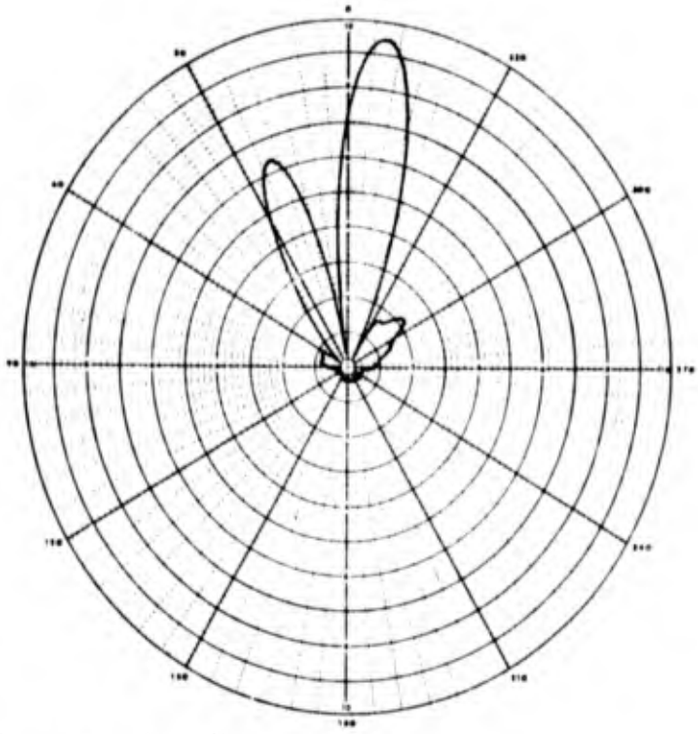

(a) Plane: $\phi = 0^{\circ}$

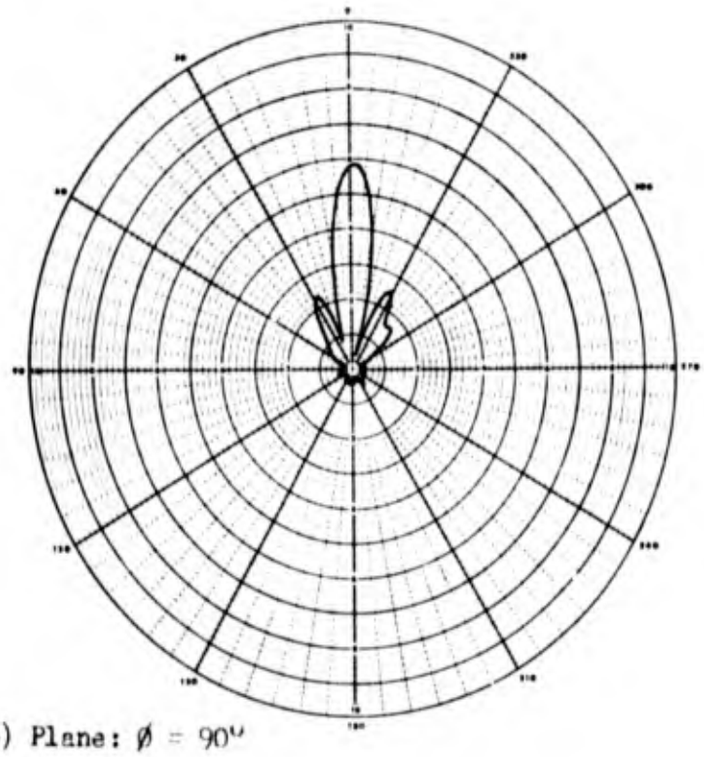

(b) Plane: $\phi = 90^{\circ}$

Figure 37. Sum of sum and difference patterns of four element array. 1300 mc.

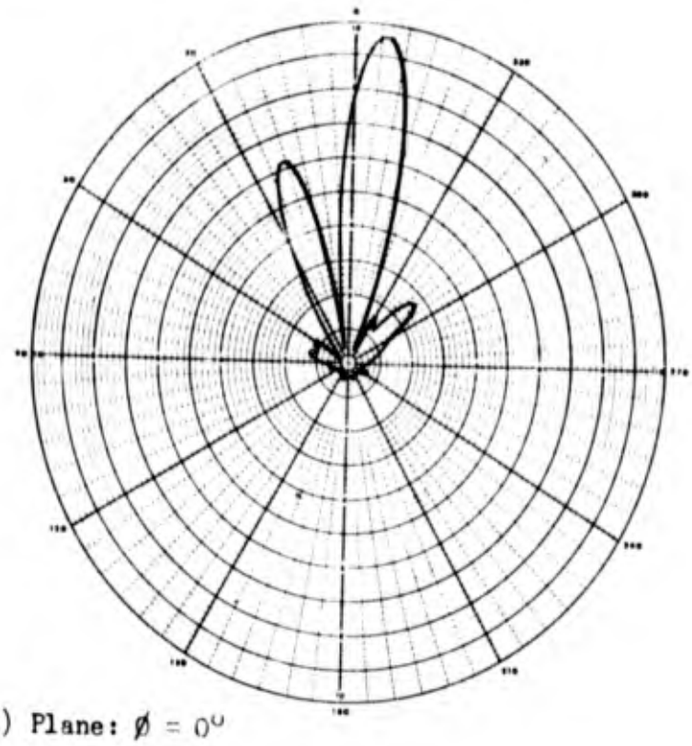

(a) Plane: $\phi = 0^{\circ}$

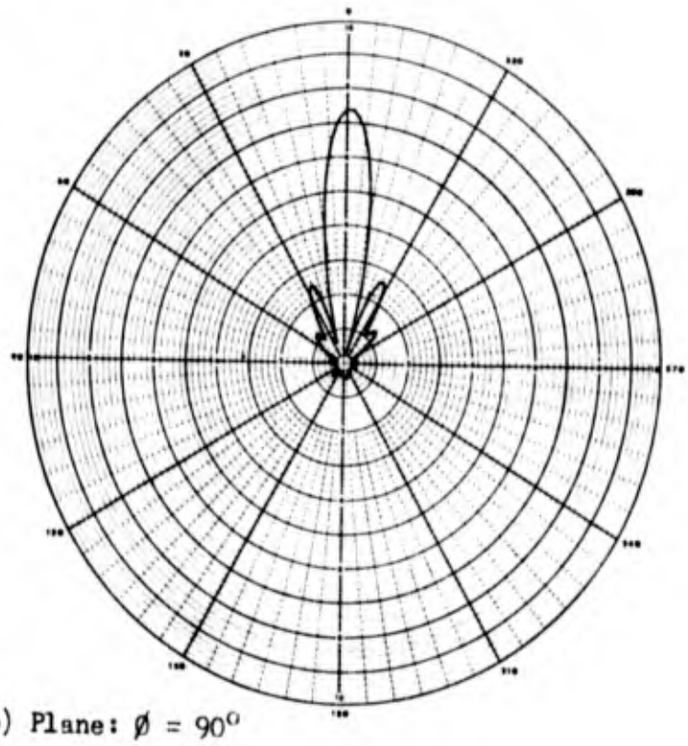

(b) Plane: $\phi = 90^{\circ}$

Figure 38. Sum of sum and difference patterns of four element array. 1400 mc.

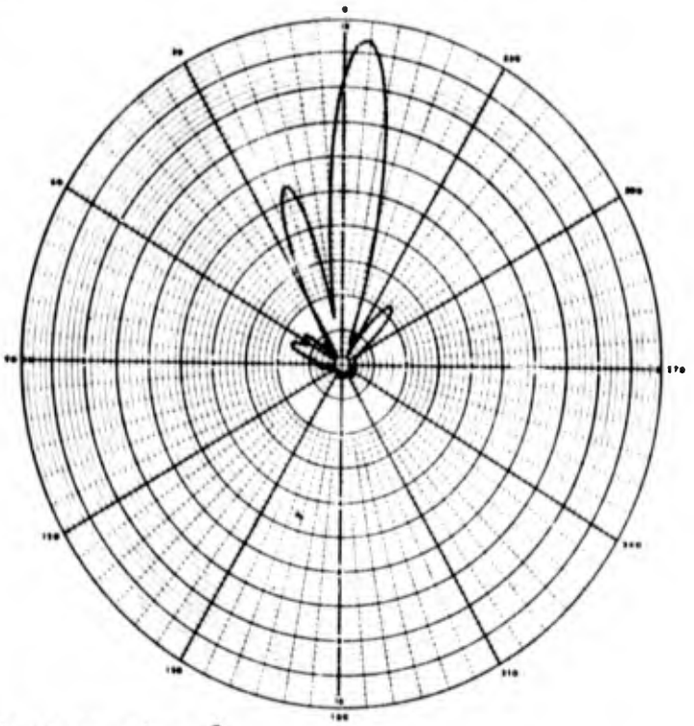

(a) Plane: $\phi = 0^{\circ}$

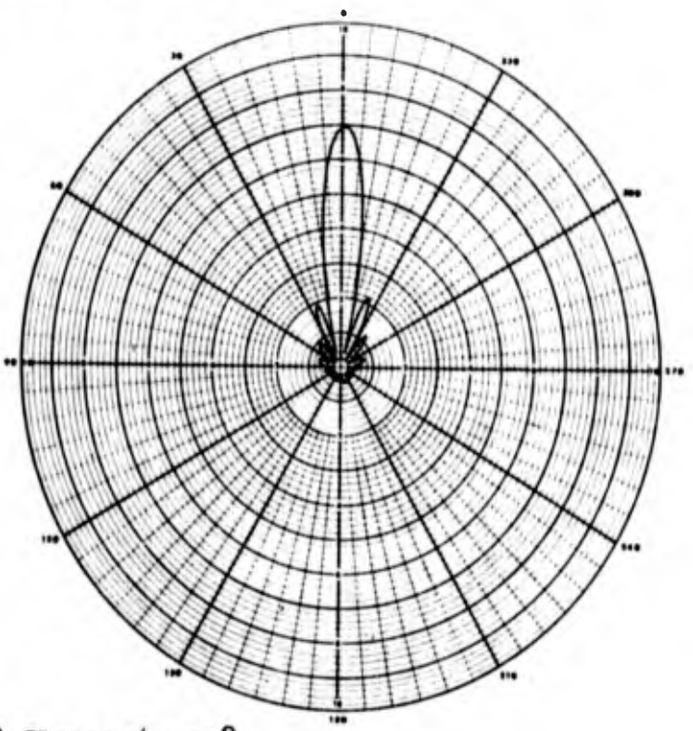

(b) Plane: $\phi = 90^{\circ}$

Figure 39. Sum of sum and difference patterns of four element array. 1500 mc.

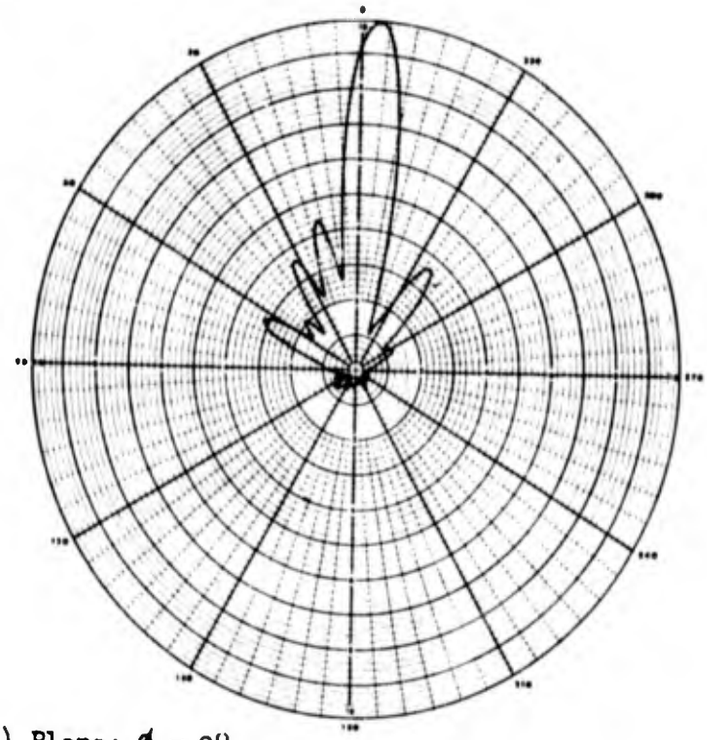

(a) Plane: $\phi = 0^{o}$

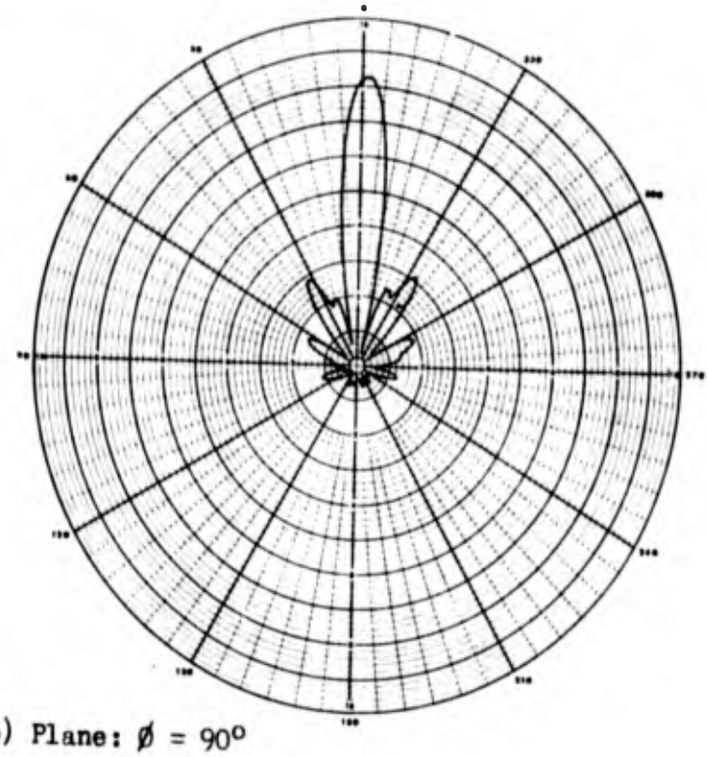

(b) Plane: $\phi = 90^{o}$

Figure 40. Sum of sum and difference patterns of four element array. 1600 mc.

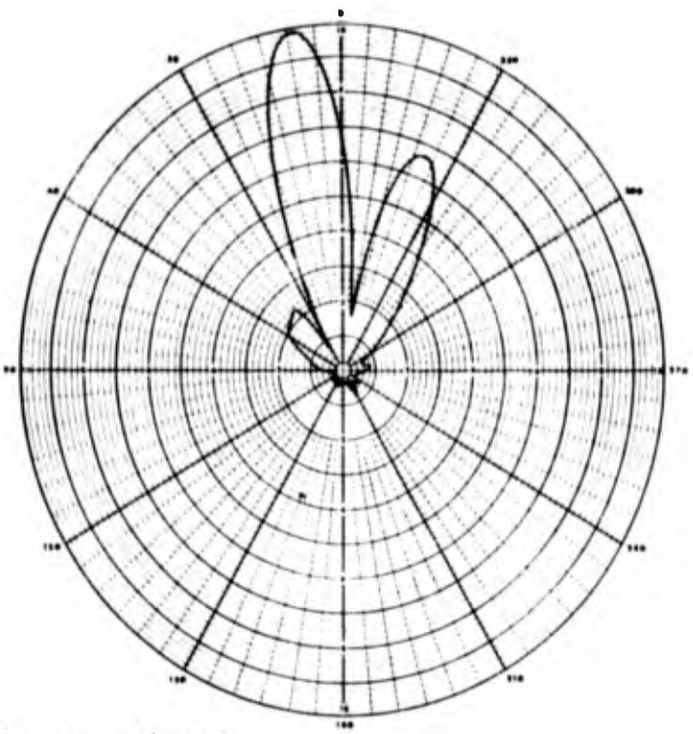

(a) Plane: $\phi = 0^{\circ}$

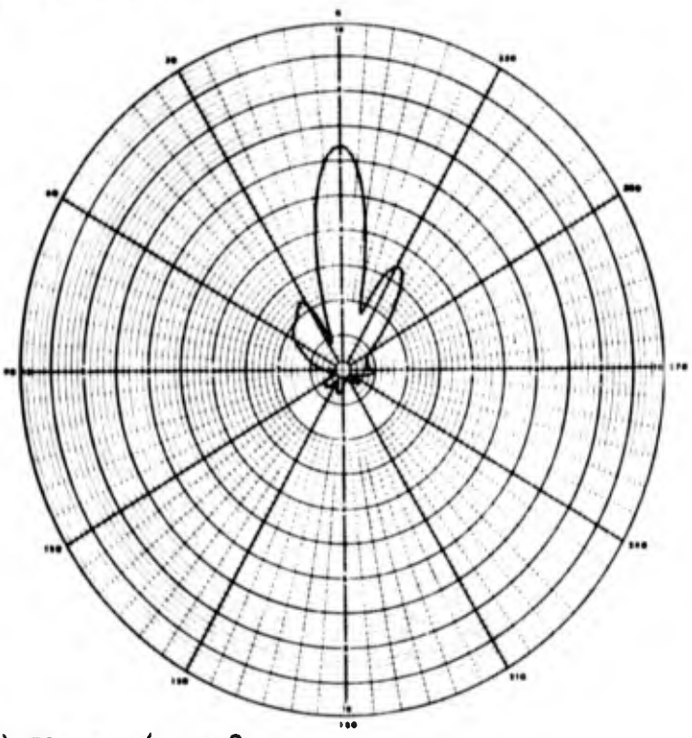

(b) Plane: $\phi = 90^{\circ}$

Figure 41. Difference of sum and difference patterns of four element array. 1200 mc.

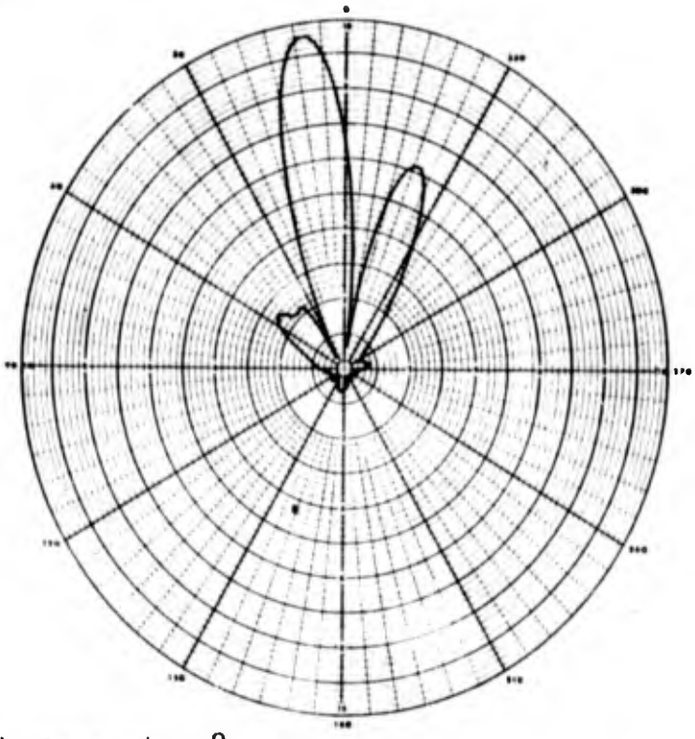

(a) Plane: $\phi = 0^{o}$

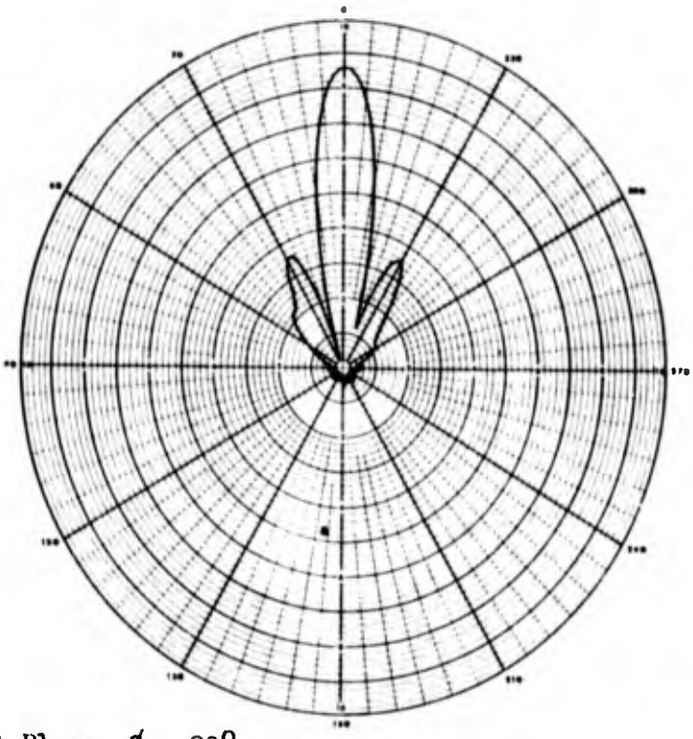

(b) Plane: $\phi = 90^{o}$

Figure 42. Difference of sum and difference patterns of four element array. 1300 mc.

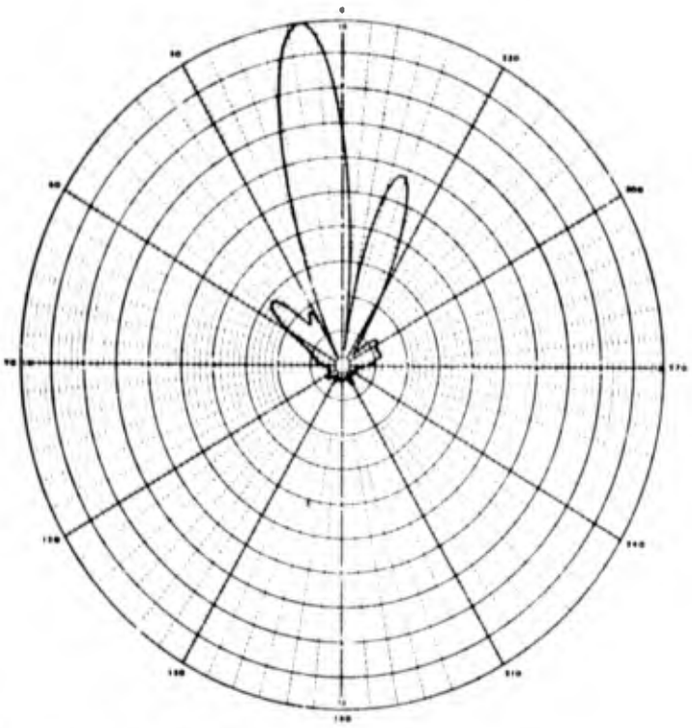

(a) Plane: $\phi = 0^{\circ}$

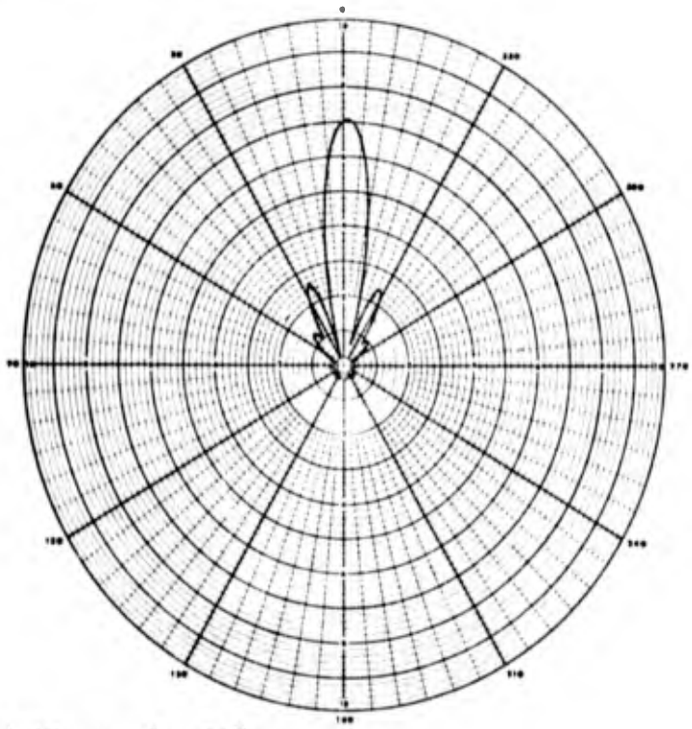

(b) Plane: $\phi = 90^{\circ}$

Figure 43. Difference of sum and difference patterns of four element array. 1400 mc.

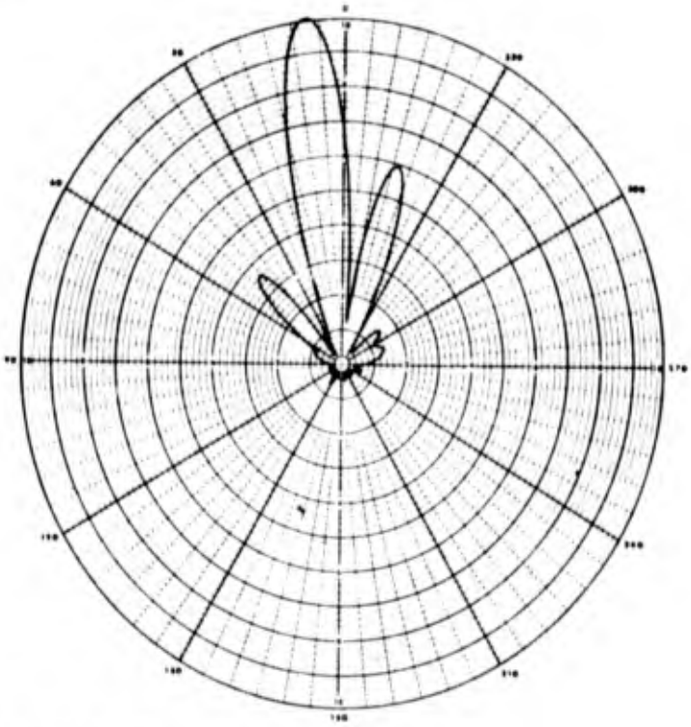

(a) Plane: $\phi = 0^{o}$

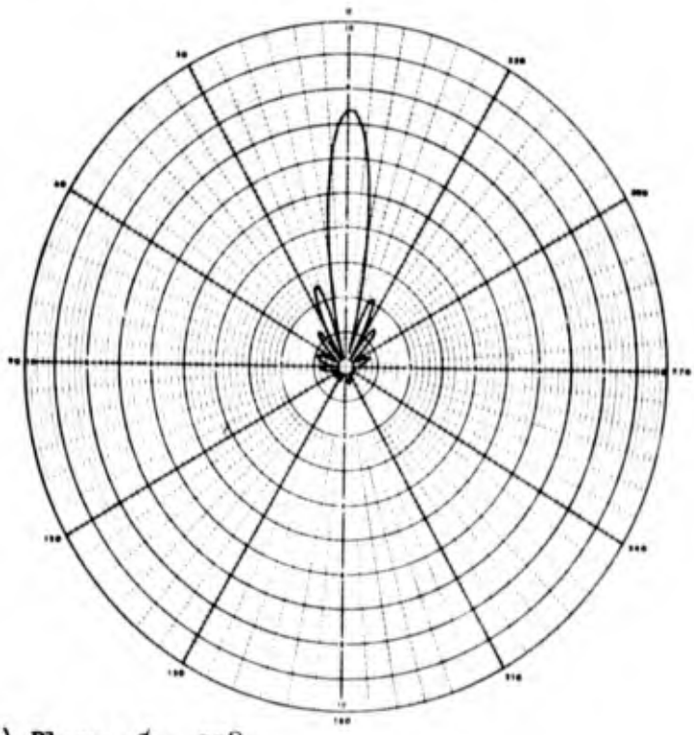

(b) Plane: $\phi = 90^{o}$

Figure 44. Difference of sum and difference patterns of four element array. 1500 mc.

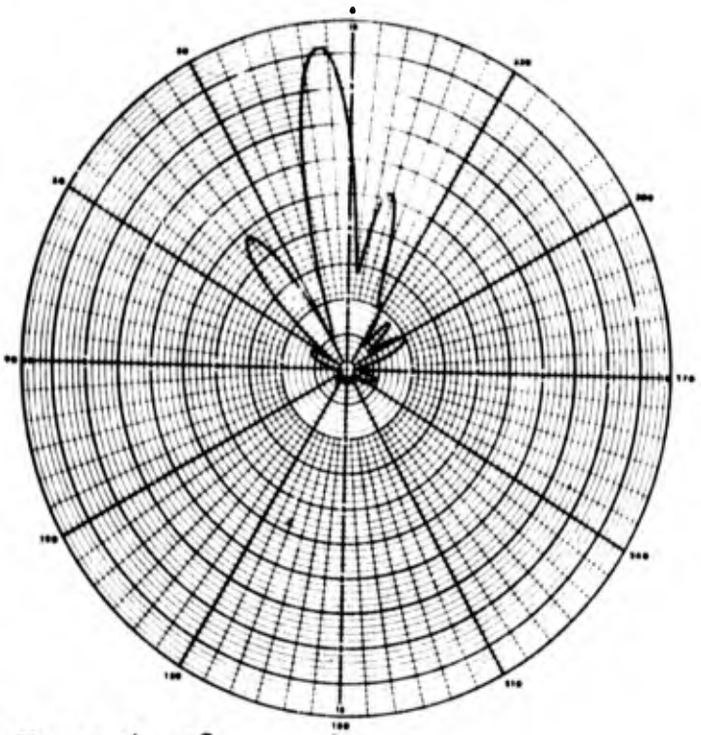

(a) Plane: $\phi = 0^{\circ}$

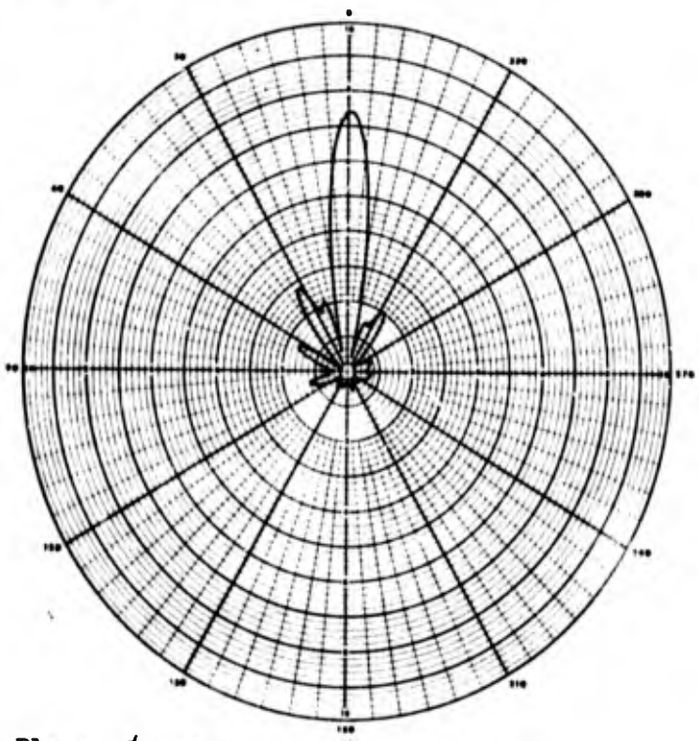

(b) Plane: $\phi = 90^{\circ}$

Figure 45. Difference of sum and difference patterns of four element array. 1600 mc.

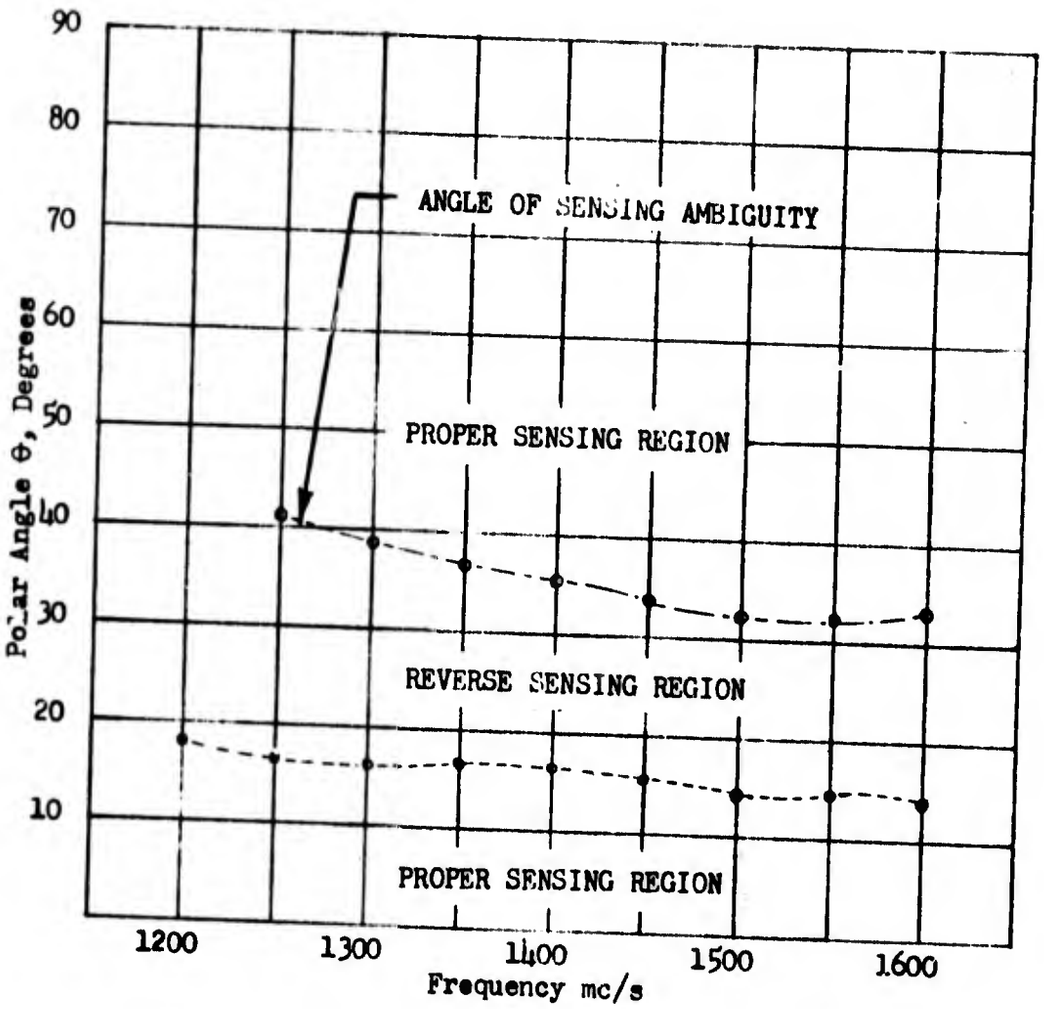

Figure 46. Direction finding sensing regions.